A revised calibration of the interferometric mode of the CryoSat-2 radar altimeter improves ice height and height change measurements in west Greenland.

5 Laurence Gray[1], David Burgess[2], Luke Copland[1], Thorben Dunse[3], Kirsty Langley[4], Geir Moholdt[5].

[1]Department of Geography, Environment and Geomatics, University of Ottawa, Ottawa, K1N 6N5, Canada
[2]GSC NRCan, Ottawa, K1A 0E8, Canada
[3]Department of Geosciences, University of Oslo, 0316 Oslo, Norway
[4]Asiaq, Greenland Survey, 3900 Nuuk, Greenland
10 [5]Norwegian Polar Institute, NO-9296 Tromso, Norway

Correspondence to: Laurence Gray (laurence.gray@uottawa.ca)

Abstract. We compare geocoded heights derived from the interferometric mode (SARIn) of CryoSat to surface heights from calibration-validation sites on Devon Ice Cap and West Greenland. Comparisons are included for both the heights derived from the first return (the 'point-of-closest-approach' or POCA) as well as heights derived from delayed waveform returns

15 ('swath' processing). While swath processed heights are normally less precise than edited POCA heights, e.g., standard deviations of ~3 m and ~1.5 m respectively for the West Greenland site, the increased coverage possible with swath data complements the POCA data and provides useful information for both system calibration and improving digital elevation models (DEMs). We show that the pre-launch interferometric baseline coupled with an additional roll correction (~0.0075° ±0.0025°), or equivalent phase correction (~0.0435 ±0.0145 radians), provides an improved calibration of the interferometric

20 SARIn mode.

We extend the potential use of SARIn data by showing the influence of surface conditions, especially melt, on the return waveforms, and that it is possible to detect and measure the height of summer supraglacial lakes in West Greenland. A supraglacial lake can provide a strong radar target in the waveform, stronger than the initial POCA return, if viewed at near normal incidence. This provides an ideal situation for swath processing and we demonstrate a height precision of ~ 0.5 m for

25 two lake sites, one in the accumulation zone and one in the ablation zone, which were measured every year from 2010 or 2011 to 2016. Each year the lake in the ablation zone was viewed in June by ascending passes and then 5.5 days later by descending passes which allows an approximate estimate of the filling rate. The results suggest that CryoSat waveform data and measurements of supraglacial lake height change could complement the use of optical satellite imagery and be helpful as proxy indicators for surface melt around Greenland.

1 Introduction

Temporal change in ice sheet surface elevation derived from satellite altimeters has been used in mass balance estimates and the associated contribution to sea level rise, (e.g. Davis and Ferguson, 2004; Rémy and Parouty, 2009; Shepherd et al., 2012; Hurkmanns et al., 2014; Zwally et al., 2015). Satellite radar altimeters have traditionally operated at Ku band (~ 13 GHz) and used parabolic transmit/receive dish antennas with a diameter of ~ 1 m, so that the main beam illuminates an area beneath the satellite with a diameter of ~15 km and area of ~180 km^2. With a typical bandwidth of ~ 300 MHz the range resolution is ~ 50 cm and, as delay time increases beyond the point at which the first surface returns are received, an increasing area contributes to the received signal. These returns are termed 'pulse limited', with the initial signal originating from the area within the main beam closest to the satellite, often referred to as the 'Point-Of-Closest-Approach' (POCA). With these parameters, the diameter of the initially sampled POCA area over the ocean is ~ 1.2 - 1.5 km, but this isn't necessarily the case over glacial ice. The initial area contributing to the leading edge of the waveform (the delay time variation in received power) over an ice cap or ice sheet depends on the topography. All we know is that it must originate from somewhere within the area illuminated by the main antenna beam and that part of the POCA surface area must be orthogonal to the incident wave. Considering the large variability in ice cap topography and surface conditions, it is not unexpected that the waveforms from glacial ice will vary significantly in shape and power. The fact that the geographic position of the POCA is, a priori, unknown is one of the major problems in traditional radar altimetry and methods to get around this limitation have been studied extensively (Brenner et al., 1983, Bamber, 1994, Brenner et al., 2007, Hurkmanns et al., 2012, Levinsen et al., 2016).

The European Space Agency (ESA) launched CryoSat as the first in their 'Earth Explorer' series of satellites, which are designed to explore and demonstrate new techniques and methods in Earth observation. As such, CryoSat was designed to include a new mode of operation to address some of the limitations of traditional radar altimetry when used over sea ice, ice caps, and ice sheet margins. The new approach uses bursts of pulses in which the frequency of the pulses within each burst is high enough that coherent Doppler processing can be used to focus the energy in the along-track direction, and ultimately create a footprint for which the along-track position is known, but the footprint centre can still be displaced from the sub-satellite track dependent on the cross-track slope. The along-track processing approach is referred to as 'Delay-Doppler' and was pioneered by Raney (1998). The suggestion that cross-track interferometry could solve the cross-track footprint position problem in radar altimetry is due to Jensen (1999). For glacial terrain the new 'SARIn' mode of operation provides a relatively small geocoded footprint which allows, for the first time, a systematic comparison of satellite radar altimeter elevations with surface heights from surface and airborne campaigns.

The first CryoSat satellite equipped with the Synthetic Aperture Interferometric Radar Altimeter (SIRAL) was launched in 2005 but failed to enter orbit. A replacement satellite was launched in 2010 and, as of March 2017, is still operating satisfactorily, almost four years beyond its design life. CryoSat operates in three modes: a conventional low resolution mode (LRM) which is used over oceans and the interior of Antarctica and Greenland, a synthetic aperture mode (SAR) for use over sea ice, and the interferometric SARIn mode over all the other glacial ice areas on Earth. A comprehensive description

of CryoSat is given by Wingham et al. (2006). Here we are concerned primarily with SARIn mode calibration and with demonstrating some unique capabilities of this new mode of satellite radar altimetry. These depend primarily on the ability to geocode the position of the relatively small footprint.

After the initial commissioning phase of the satellite in spring and summer 2010, intermediate and final products were
5 available from ESA. For glacial ice the ESA level 2 (L2) product contains the position and height of the geocoded POCA positions. An additional L2i product is available which contains the same geocoded height solution as the L2 product, but also information on the waveform which can be used to help eliminate poor data and solutions. An intermediate product (L1b) has also been made available which includes the waveform power, phase, coherence, satellite position and velocity, etc., and all the corrections and timing information necessary to calculate the position and height of the POCA footprint. This
10 has been useful to those users wishing to study processing techniques; for example, by having access to the intermediate L1b product it has been possible to demonstrate that the returns which are time delayed beyond the initial POCA position can be used in areas with suitable cross-track slopes to create 'swath processed' elevations (Gray et al., 2013). Initially, airborne data had been used to demonstrate the possibility of swath mode processing of Delay-Doppler data (Hawley, et. al., 2009). The L1b products have also been used in several studies of change in Antarctica and Greenland (e.g. Helm et al., 2014,
15 Nilsson et al., 2016, Christie et al., 2016, Smith et al. 2016), smaller Arctic ice caps (Gray et al. 2015, Foresta et al., 2016), and lake height (Kleinherenbrink et al. 2014). In these studies, the authors claim improvements in the results over the standard level 2 product, due to the specialized processing.

Three versions of the various CryoSat products have been distributed by ESA since commissioning; these are the so-called baseline A, B and C products. Details of the improvements can be found through the ESA Earth Online web site devoted to
20 the CryoSat mission (https://earth.esa.int/web/guest/missions/esa-operational-eo-missions/cryosat). Here we have used only the latest baseline C products, particularly because the waveforms in these products span a range window distance of ~ 240 m, twice the distance available in the baseline B products. Some comparisons are also made between results derived from the baseline C L1b files and those provided in the L2 products.

In this study we use CryoSat and surface height data from two well-studied sites in the Canadian Arctic and Greenland to
25 improve the calibration of the SARIn mode. Further, we show that the waveforms do change significantly with surface melt and that it is possible to detect the formation of supraglacial lakes. By using a modified swath processing scheme, we also show that it is possible to measure lake height and height change.

2 Methods

Our processing methods were described in Gray et al. (2013) and Gray et al. (2015). The current Matlab processing provides
30 both POCA and swath mode results, and here we note any changes since the earlier work. The method to generate POCA heights are comparable to those described in Helm et al. (2014), Nilsson et al. (2016) and Smith et al (2016), and were

motivated by similar concerns, particularly the performance of the L2 'retracker': this is the algorithm designed to find the position of the POCA return in each waveform.

The Delay-Doppler processing (Raney, 1998) for the SARIn mode of CryoSat is described in Wingham et al. (2006) and Kleinherenbrink et al. (2014). In this method 64 pulses are used in each transmitted burst and fast Fourier transform processing is used to create 64 unfocussed beams so that, with appropriate superposition of results from a sequence of bursts, multiple 'looks' can be averaged for each ground footprint. In practice there are less than 64 looks contributing to each waveform in the L1b file, normally ~ 57. In the along-track direction the footprints are separated by ~ 280 – 300 m and the resolution is ~ 380 m (Bouzinac, 2015). In the cross-track direction the footprint size is dictated by the cross-track slopes and by any smoothing of the waveform in the processing. The position of the POCA footprint derived from each waveform will be in the plane including the satellite position, and the lines defined by the cross-track and nadir directions. The POCA area will be centred on the closest point in the intersection of this plane with the terrain surface so that when ascending and descending orbits cross the two POCA footprints will not be the same when there is a cross-track slope. Consequently, it is not appropriate to compare results from the interpolated orbital cross-over point. The L1b files contain two echo scaling parameters for each waveform which allow a calibration of the waveform power to watts, the logarithmic (dB) values used in the results are then with respect to 1 watt.

2.1 Selecting the POCA position from the SARIn waveform

If the altimeter response from terrain was 'predictable' it would be beneficial to use the complete waveform in the estimation of the position in delay time of the surface, and this is the basis of the ESA L2 processing. However, our experience with the L1b SARIn waveforms over glacial ice shows that the shape and magnitude of the waveform can vary significantly, even in one area at one time (see examples in section 4). The average return power as a function of delay time from the first surface sample will vary with the illuminated surface area, the reflectivity of the surface and any near surface layering on the ice cap. The cross-track slope and fixed sampling in delay time (3.125 ns) defines the basic cross-track footprint size so that the waveform shape beyond the POCA depends primarily on the variation in topography in the cross-track direction. This is essentially independent of the position of the POCA, hence our decision to estimate the POCA position based on the first significant leading edge in the waveform. Our approach (Gray et al. 2015) uses the point of inflexion (maximum slope) on the first significant waveform increase, and is similar to that adopted by Nilsson et al. (2016) and Smith et al. (2016). Helm et al. (2014) used a threshold level of the first significant leading edge for their work in Greenland and Antarctica, following the work of Davis (1997) who advocated a threshold retracker to minimize the dependency on varying microwave penetration into, and backscattering from, various snow-firn-ice layers. The importance of the cross-track footprint size in dictating the shape of the waveform has been demonstrated by the success of the straightforward waveform simulation based primarily on topography shown in Gray et al. (2013).

Although the L1b waveforms already represent averaged values, some additional smoothing has been done on the complex waveform data. The low-pass filter uses a 3 dB width of ~ 4 samples and is designed to avoid introducing any bias in the waveform phase. Smoothing the SARIn waveform data is performed only in the range direction with a relatively small impact on the cross-track footprint size (Gray et al. 2015), and none on the along-track resolution. The resulting reduction in phase noise improves the POCA footprint geocoding, as the phase provides the cross-track look angle. It is not appropriate to average any of the L1b waveform data in the azimuth direction because there can be jumps in the delay time to the first waveform sample. The processing steps to generate geocoded heights are described in Gray et al. (2015) using the results of the calibration described in section 3 below. Solutions are derived for the phase at the estimated POCA position in the waveform, and for this phase $+2\pi$ and -2π. Comparison with the height of the reference DEM is used to select the most likely of the three solutions. Some waveforms are not used for POCA generation. This can occur for various reasons; the coherence at the POCA point is less than 0.7; the power for the average of the first 5 waveform values is too high (> -150 dB, for baseline C); the ratio of the maximum waveform power to the average of the first 5 values is too low (< 6 dB), or there is not a clear leading edge in the waveform. These criteria are rather arbitrary and may be changed for different sites, depending on the results. For example, we found that using a more stringent POCA coherence requirement improved the overall results for the west Greenland site.

2.2 Swath mode processing

The techniques used to process the returns delayed beyond the POCA position are essentially as described in Gray et al. (2013). In that work the bias errors associated with the uncertainty in the baseline roll angle (Galin et al., 2013) were reduced by comparing the derived E–W slope on the western flank of Devon Ice Cap with the reference data slope, and changing the baseline roll angle to minimize this error. This step has not been undertaken here as it presumes a good quality reference DEM which is not necessarily available.

Waveform smoothing can lead to a situation in which results may be oversampled in the cross-track direction. The swath processed results from any one waveform will form a straight line in the cross-track direction and the final samples in cross-track are generated by binning and averaging the results in segments of the cross-track line. The separation between ground-range cross-track samples is nominally ~100 m. Criteria for minimum values of the filtered coherence and returned power are set, and are usually ~0.84 and -150 dB, respectively, for baseline C data. The phase unwrapping and ambiguity checking method is similar to that described by Smith et al. (2016).

The swath processing of the summer CryoSat data for supraglacial lake height (section 4.2) omitted the cross-track binning stage and produced an elevation for each sample in the waveform. Only heights derived from waveform samples with phase values equivalent to small look angles (< ~ 0.2°), high power (> ~ -140 dB), and high coherence (> 0.95) were used. These minimum values virtually guarantee that there will be a small contribution from the range ambiguous zone, and that phase unwrapping or ambiguity checking is unnecessary. The resulting geographic positions were compared to the best available

visible imagery, usually Landsat 8 images, and north, south, east and west boundaries around the lake feature were set. The resulting height estimate was then obtained by averaging all estimates within the lake boundary.

2.3 Measuring the height difference between the reference surface and CryoSat heights.

We used two methods to compare the derived CryoSat heights with the surface reference data. For Devon Ice Cap the

5   reference data included inter-calibrated snowmobile-based differential GPS transects, and airborne scanning laser altimeter data from both the NASA Airborne Terrain Mapper (ATM; Krabill et al., 2002, Krabill, 2014) and the TUD ALS (https://earth.esa.int/documents/10174/134665/ESA-CryoVEx-ASIRAS-2014-report) systems. For the Greenland site, we have relied on the ATM data collected on NASA IceBridge flights. The first method stepped through all the CryoSat results and searched for reference heights within 400 m of the centre of the CryoSat footprint. The height differences between the

10   CryoSat and reference heights were corrected for the slope between the centres of the two footprints using interpolation with the reference DEM. If there were many reference values, as can be the case for the west Greenland site, then a second simpler method was used: a search was made for reference points within 50 m and the height differences were tabulated and averaged without the slope correction stage. Virtually all the reference height data for both sites were obtained under cold conditions in April or early May and we assumed that any accumulation or change in the backscatter conditions between

15   January and mid-May would lead to a relatively small change in the CryoSat height. This provided the rationale for comparing all the CryoSat results from the January to May passes with the April or May reference height data.

2.4 Estimating height errors in the CryoSat data

Ku band radar waves can penetrate the surface and the CryoSat-to-surface height bias will vary depending on the conditions of the surface and near surface (Gray et al., 2015; Nilsson et al., 2015). Consequently, we use the standard deviation of the

20   height differences about the mean height difference as the primary measure of the quality of the CryoSat measurements. The relatively small error in the ATM or ALS laser surface heights (~ 20 cm, Krabill et al., 2002) is ignored, and any impact due to the difference in the footprint size is not considered.

When estimating the height errors for the supraglacial lakes it is not appropriate to quote the standard error (standard deviation divided by the square root of the number of samples averaged), because the samples will not be independent and

25   there is the possibility of small bias error in the result. The errors were therefore estimated on a case-by-case basis by looking at any cross-track slope across a lake feature, using the standard deviation itself, and checking independent estimates from ascending and descending passes over the same feature. The standard deviation about the mean was typically ~0.5 m, and the mean difference between the ascending and descending passes over the same accumulation zone lake feature in August was ~ 0.25 m. Table 1 includes the error estimates from two lakes and shows that relatively good precision can be

30   achieved for these strong targets, better than the potential error for individual POCA estimates.

3 Results: SARIn mode calibration

The key parameters for SARIn mode geocoding are the range to the surface, and the satellite look angle between the normal to the WGS84 ellipsoid and the footprint centre in the cross-track plane. The former involves consideration of timing and the retracker algorithm for the POCA results, but it is the latter which requires careful calibration for both POCA and swath mode results.

The satellite look angle, α, is related to two other angles through:

$$\alpha = \beta - \delta \tag{1}$$

Where β is the interferometric angle defined below, and δ is the roll angle of the interferometric baseline, all defined in the cross-track plane containing the line normal to the WGS84 ellipsoid. The angle β is related to the interferometric phase through (Galin et al., 2012):

$$\beta = -\mathrm{asin}(\chi/kB) \tag{2}$$

Where χ is the phase provided in the L1b file, k is the wavenumber, B is the length of the interferometric baseline, and the Cryosat altimeter transmits through the left antenna and receives from both. The sense of the look and interferometric angle is as follows: For zero roll an observer siting on the CryoSat satellite facing in the direction of motion with their feet pointing towards the Earth will 'see' a footprint to the right of the sub-satellite track when the look angle α is positive. The roll angle δ is also provided in L1b files. For the same observer configuration, a positive roll angle corresponds to the left antenna being higher than the right hand one.

Any bias in the look angle, $\Delta\alpha$, can then be related to biases in the baseline; ΔB, phase; $\Delta\chi$, and roll angle; $\Delta\delta$, through:

$$(\alpha + \Delta\alpha) = -asin\left(\frac{(\chi + \Delta\chi)}{k(B + \Delta B)}\right) - (\delta + \Delta\delta) \tag{3}$$

Using the approximations that $\sin(x) = x$ for small x and $B \gg \Delta B$, leads to an expression for the bias in roll angle as:

$$\Delta\alpha = -\frac{\Delta\chi}{kB} + \frac{\chi}{kB}\left(\frac{\Delta B}{B}\right) - \Delta\delta \tag{4}$$

The CryoSat satellite and processing chain contains careful controls which should minimize any extraneous inter-channel phase shift $\Delta\chi$ on the satellite (Bouzinac, 2015). Even if a residual phase bias exists, due perhaps to an uncompensated path length difference between the two receivers, it can be expressed in the same form as the roll-angle correction $\Delta\delta$ and the two can be considered together. The second term in equation (4) reflects the possibility of a bias between the actual and pre-launch measurement of the interferometric baseline; the distance between the two antenna phase centres. This was part of the post-launch SARIn mode calibration carried out by Galin et. al. (2013). This work used results from satellite roll manoeuvres over mid-latitude ocean tracks to show that the interferometric angle should be scaled by a factor of 0.973 ± 0.002, which is equivalent to scaling the baseline by a factor of 1.0277. The third term in Eq. (4), the uncertainty in the baseline roll angle $\Delta\delta$, is important because the baseline roll angle is derived from one of three star trackers mounted on a support bench on the satellite. Galin et al., (2013) identified a problem with the reported roll angle and suggested that this was due bending of the

support bench under a changing thermal environment. However, recent work by ESA (Scagliola et al., 2017) showed that the roll-angle problem arose, at least partly, because of an error in processing the star-tracker data. Consequently, there is currently an unknown bias in the reported value of the baseline roll angle which can vary pass-to-pass. In the following sections, we use SARIn data over well-documented glacial ice to investigate any residual bias in the roll angle provided in the L1b files, and to study the influence of changing the baseline length in processing L1b files.

3.1 Calibration test sites

We used data from two sites, the western flank of Devon Ice Cap (Fig 1), and an area in western Greenland including the Jakobshavn Glacier (Fig. 2), as both have excellent reference surface height data. Our calibration approach depends on the presence of a predominantly east-west slope which is why the test area in Fig. 1 is limited in the north-south direction. By using terrain with an east-west slope we obviate the necessity for roll-tilting the satellite. Figure 3 illustrates the difference in the slopes for the two test sites. The significant increase in slope variation in the west Greenland site represents a more challenging situation for satellite radar altimetry than the more modest slope variation on the western flank of Devon Ice Cap, and this is the reason we have concentrated on comparing the results from these two test sites.

3.2 Calibration based on data from Devon Ice Cap

The western portion of Devon Ice Cap has suitable cross-track slopes for swath mode height estimation for both ascending and descending passes, and this area was used in the demonstration of swath mode processing (Gray et al. 2013). While the possible range of average cross-track slopes can be ~0.5° to ~2°, here we have restricted the use of results to E-W slopes of ~0.7° - 1.5° over a distance of >5 km as this range generally provides a better suppression of the ambiguous range contribution. Figure 1 shows the positions of the spring 2011 surface height reference data obtained from NASA and ESA supported overflights, and from surface snowmobile dGPS transects, all superimposed on a colour representation of the reference DEM. The sub-satellite tracks of 15 CryoSat passes are also shown. Results from all the passes in this time period were compared to the reference surface heights as conditions on Devon Ice Cap change little between January and May, and we assume that any change in surface height or change in the bias between the surface and CryoSat height was small with respect to the error in the CryoSat heights.

The histogram of the difference between the reference and CryoSat swath mode heights obtained with the pre-launch baseline estimate (1.1676 m, Bouzinac, 2012) showed a bimodal distribution and the average bias changed between ascending and descending passes, ~-0.5 and ~2.5 m respectively. As we could find no reasonable geophysical explanation for this difference, the possibility of a roll-angle bias was investigated. If there was a roll-angle bias on an ascending pass the swath-processed height estimates would be displaced either up- or down-slope depending on the sense of the bias. However, with a descending pass and the same roll-angle bias, the results will be displaced in the opposite direction and the height bias will have the opposite sign from that obtained with the ascending pass. To investigate this effect further, all the data in this

time period were reprocessed with an additional roll-angle bias added to the value provided in the L1b file. Figure 4 illustrates the results of an experiment in which the 15 2011 passes (7 ascending and 8 descending) were each reprocessed 9 times with an additional roll correction varying from -0.02° to +0.02°. The results were then compared to the reference height data collected in early May 2011. As expected, the sense of the height difference changes between ascending and descending passes but the curves do not overlap well. While the results from the 8 2011 descending passes do cluster nicely this was not the case for the 2012 data (Gray et al. 2016), and neither year shows consistent results for the ascending pass results.

Consequently, it appears that the roll angle provided in the L1b file has a time variable bias, apparently due to a problem in processing the star-tracker data (Scagliola et al., 2017). The uncertainty in the roll angle in this example appears to be of order 0.006° or ~ 100 µradians, not inconsistent with the observations in Galin (2013). While there will be a contribution from the range ambiguous zone in swath mode processing, which could introduce a small bias, this does not appear to be the primary source of these differences. The roll-angle uncertainty, and resulting unknown bias in the baseline roll angle, appears to be a limitation to the use of swath mode heights. Note that in Fig. 4 there is essentially no slope to the plots of the height difference versus roll-angle bias for the POCA height estimates. This is direct consequence of the fact that while the POCA estimates are mapped incorrectly when there is a roll-angle error, the derived height can still be appropriate for the wrong position because the incident wave may still be essentially perpendicular to the surface (Gray et al., 2013).

The variable E-W cross-track slope also provides a suitable test area to check the phase to cross-track angle conversion dictated by the baseline (Eq. 2 above). Figure 5 illustrates the results of an experiment in which the results obtained with a phase-to-angle conversion based on the pre-launch baseline are compared to the calibration given by Galin et al. (2013). The two histograms on the left used the pre-launch baseline while the histograms on the right used the angle scaling from Galin et al. (2013). Figure 5C shows the bimodal distribution referred to earlier, and Fig. 5A shows the improved results with a significantly narrower error distribution when a bias of 0.0075° is subtracted from the roll angle provided in the L1b file. The uncertainty in this additional roll bias has been estimated as ±0.0025°. When the phase-to-angle is scaled by 0.973 (Fig. 5B and 5D) the results show a broader distribution and poorer results.

3.3 Calibration based on data from west Greenland

We use IceBridge data from an area in central western Greenland (Fig. 2, insert) including the Jakobshavn Glacier, an area which has shown significant surface height loss in recent years due to both change in output flux and surface mass balance (Joughin et al., 2008, Qi and Braun, 2013), and has excellent reference surface height data (Krabill et al. 2002, Krabill 2014).

Figure 2 illustrates the positions of the reference surface height data obtained from the four NASA IceBridge flights flown on Mar. 31, and Apr. 6, 7, and 23, 2011 superimposed on a black and white representation of the GIMP DEM (Howat et al. 2014). This DEM was used as the reference DEM for all the CryoSat processing in this area. Data from the ATM L2 files

have been used for this work and compared with height results from all the CryoSat passes between 16 Feb. and 23 April.

It is important to recognize the differences in this test site in relation to that on Devon Ice Cap. The two profiles in Fig. 3 show that even in the accumulation area of this part of west Greenland the slope variation is much larger than on the EW profile interpolated from the airborne laser altimeter flown over of Devon Ice Cap. The difference is also very apparent in the

5   CryoSat results: Figure 6 compares two image representations of the waveform power for 22 km segments of the Feb. 7 2011 ascending pass over Devon Ice Cap and the April 21 2011 descending pass over the west Greenland test site. For the ascending pass over Devon Ice Cap the POCA position will be on the left close to the beginning of the 240 m range window, as indicated by the stronger return signals in red. However, for the west Greenland site the peak return is often in the middle of the waveform. The difference in the signals may be influenced by the different conditions but it is clear that the dominant

10 reason for the differences in waveforms is due to differences in the cross-track slopes. The larger slope variation in west Greenland clearly influence the CryoSat returns, and the waveform shape is now much more variable than those from the Devon test site. This situation favours a retracker which looks for the first significant leading edge, rather than one that assumes a particular model for the waveform and then fits the waveform to that model, as is the case for the ESA L2 SARIn product. Some details of the retrackers used in the baseline C L2 products are given in Buffard (2015).

15 Figure 7 compares the results obtained with our geocoding and that obtained with CryoSat L2 retracker. Our processor picks out the POCA position satisfactorily (black dots on Fig. 7A) and leads to the mapping solution shown in Fig. 7B. The positions of the CryoSat L2 solutions are shown in Fig. 7B as purple dots, and are often different by many kilometres. The solutions are close only when the waveforms show a clear maximum close to start of the waveform (e.g. at ~ 70.05 N). Using the position of the L2 solution, the off-nadir look angle and equivalent phase can be calculated. Then the position in

20 the waveform with that phase is identified and marked as purple dots in Fig. 7A. This shows that the L2 retracker normally does not identify the point-of-closest-approach correctly, primarily because of the strong peaks in middle of the waveform.

In comparing our CryoSat POCA height results with the ATM surface height results we found that the results here were not as precise as those obtained over the Devon test site. However, when slightly more stringent editing was used, in particular by increasing the minimum POCA coherence requirement to 0.8 from 0.7, then the results were improved. The histograms of

25 the ATM minus CryoSat heights for the 2011 spring data are shown in Fig. 8. Again the poor results from the baseline C CryoSat L2 files are apparent (Fig 8A), particularly the much larger number of height errors greater than 20 m. Results from exactly the same waveforms have been used in this comparison, as the L2 results were removed for those waveforms already removed through the L1b editing. While it is unfair to compare results from an operational algorithm which must work everywhere to one which can be tuned for different areas and includes editing based on the coherence and the return power,

30 it is fair to say that the current L2 retracker is inherently unsuitable for the west Greenland site. The L2 results are better in other areas, such as the ridges on Austfonna, ice rises and ice shelves in Antarctica, and parts of the Devon Ice Cap. In these areas the waveforms show a more consistent shape and the dominant return is close to the start of the waveform.

The comparison between results obtained with the angle scaling factor from the Galin et al. (2013) calibration (Fig. 9A and C), and without (Fig. 9B and D), mirrors the results discussed in the previous section for Devon Ice Cap. The results imply that the pre-launch baseline coupled with an additional roll-angle offset (or equivalent phase shift) improves the results for both west Greenland and Devon Ice Cap.

5   There is an important difference in the results for this test site in relation to Devon. For Devon, the ATM - POCA height difference was essentially independent of the roll-angle offset between -0.02° and 0.02° (Fig. 4), but this was not the case for the west Greenland site. A comparison of the average ATM - POCA height difference over 16 passes as a function of the additional roll-angle bias (Fig. 10A) shows that the CryoSat POCA height is not independent of the roll-angle bias but increases for both positive and negative bias errors from a value of ~0.0075° ±0.0025°. As the CryoSat results are mapped

10   incorrectly in the cross-track direction, the larger cross-track slopes imply that the distance in the cross-track direction which is essentially orthogonal to the incident wave is smaller in west Greenland than for the relatively smooth surface of western Devon Ice Cap. Consequently, this will lead to a CryoSat POCA height error as the mapping process takes the centre of the footprint outside the region which is orthogonal to the incident wave. Figure 10B shows the variation in the standard deviation of the swath mode ATM - CryoSat heights for each pass (dotted lines), and the average over all 16 passes (black

15   line). The offset in the position of the minimum from zero roll-angle bias also supports the contention that on average there is a difference between the actual baseline roll angle and the value reported in the L1b file based on one of the 3 star trackers, or that there is an equivalent phase shift. For batch processing, we have used the L1b roll angle minus 0.0075°, but this may change with more experience with the bias.

There is another discrepancy in these results that warrants explanation. From Fig. 9A we see that the average ATM - POCA
20   height difference is -0.16 m, but with the same waveform data the height difference from swath mode processing is +0.91 m (Fig. 9C), so that the two processing methods are giving average heights different by 1.07 m. With the Galin et al. (2013) calibration the discrepancy is even worse; 2.52 m. Further, there is an apparent discrepancy with the results from Devon Ice Cap where previously (Gray et al. 2015), and now, we see the CryoSat height as being somewhat below the physical surface. The explanation for the anomalous average ATM – POCA result for west Greenland, where the average CryoSat POCA

25   height is slightly above the surface, appears to be related to the results in Fig. 10A. If there is an error in the roll angle this will lead to an increase in detected height irrespective of the sign of the roll-angle error. This will lead to an asymmetric distribution and the mean height will be biased high. Note that the distribution in Fig. 9A is somewhat asymmetric, more so than that in Fig 9C for the swath processed data where the sign of any roll-angle error would dictate the sign of the height error. For areas like the west Greenland test site this implies that the roll-angle bias error will tend to bias the average POCA

30   height high with respect to the surface.

4 Unique capabilities of the SARIn mode.

In this section we use our methodology and revised calibration to demonstrate some unique capabilities of the SARIn mode, first by illustrating signature change with surface conditions in West Greenland, and secondly by showing that it is possible to detect supraglacial lakes in the waveform data and estimate the surface height and height change with relatively good

5   precision.

4.1 The effect of surface melt on SARIn waveforms

The influence of melt on SARIn signatures should be considered when presenting temporal height change for any region which may have undergone surface melt (Nilsson et al., 2015, Gray et al., 2015). Figure 11 illustrates one example of the influence of melt on the strength of the SARIn waveform data. The position of this July 14 2011 descending pass is shown in

10   Fig. 12A and begins at ~ 2200 m elevation, crosses the Jakobshavn Glacier at ~ 1000 m, then the elevation increases slightly before ending at ~ 1100 m. At high elevations, the returns are comparable to those obtained under cold winter-spring conditions, but at lower elevations, ~ 1700 - 1900 m, there is a decrease of ~15 - 20 dB in average waveform power. It is well known that the introduction of even a small amount of liquid water in snow dramatically alters the emissivity and backscatter (Ulaby et al., 1986). For example, a significant drop in QuikSCAT 13.3 GHz backscatter was shown to be linked

15   to melting from weather station data (Nghiem et al., 2001). The presence of water droplets in snow increases absorption, reduces the penetration depth, which in turn leads to an increase in brightness temperature and decrease in radar backscatter (Wang et al., 2016). Consequently, we associate the relatively low reflectivity at these elevations to a damp snow layer. At lower elevations (< 1600 m) not only is the average return larger but also the waveform-to-waveform variability is much higher, indicative of occasional specular reflection from a wet surface facing the radar. Also, the strongest returns in most of

20   the waveforms in this area are not from the leading edge but vary in position across the waveform so that a retracker that uses all of the waveform won't accurately measure the position and height of the POCA.

Figure 12 illustrates the average waveform power plotted against elevation for 5 descending passes (Fig. 12A) acquired during the summer of 2011. At elevations up to ~ 1300 m the June 18 pass (Fig. 12D) shows the high waveform-to-waveform variability that we suggest is due to occasional specular reflection, but this was not observed in the earlier passes

25   in April (Fig. 12B) and May (Fig. 12C). By July 14 (Fig. 12 E) the region with strong and variable power includes elevations up to ~1600 m and the August pass (Fig. 12F) shows some strong waveform returns at even higher elevations. Comparable results were obtained from the five repeat passes 369 days later in 2012, but the descending pass on July 20 2013 showed the wet snow signature at lower elevations (~ 1500 m) without any indication of occasional specular reflections. This is consistent with the relatively colder conditions at that time in 2013 with respect to both 2011 and 2012 (see e.g. Fettweis

30   2016, http://climato.be/melt-2016). The supporting material includes figures equivalent to Fig. 12 for all the years from 2012 to 2016.

4.2 Supraglacial Lakes

During summer melt around the periphery of the Greenland Ice Sheet water pools in surface depressions as supraglacial lakes (Echelmeyer et al., 1991), forming first at lower elevations and then to higher elevations as melt progresses. With increasing positive air temperatures, surface melt water will infiltrate to lower elevations so that the snow at the edges of the depression will tend to become saturated and melt before the snow in the centre of the depression. In many cases, small supraglacial streams form which will add energy to melt snow or ice where they enter the surface depression. Optical satellite imagery and DEM data have been used to study the distribution, extent, depth and drainage of these features when there is an open water surface (Box and Ski, 2007, McMillan et al. 2007, Sneed and Hamilton 2007, Liang et al., 2012, Fitzpatrick et al. 2014, Leeson, et al., 2015, Pope et al., 2016, Ignéczi et al., 2016). While Landsat and MODIS imagery have been used to estimate total lake volume of relatively large areas (e.g. Pope et al., 2016), the limitations due to clouds and atmospheric conditions hamper routine use for quantitative melt estimates. Here we demonstrate that CryoSat SARIn data can provide complementary information to that available from visible satellites by showing that measurements of surface height and height change can be derived from SARIn data over individual supraglacial lakes. SARIn data can be obtained reliably day or night and in all weather conditions, but is very limited in surface coverage.

If CryoSat passes directly over a typical unfrozen supraglacial lake one would expect a strong specular reflection which would not be at the leading edge of the waveform, as it must be surrounded by ice at higher elevations. Even if the lake has some snow cover or a partially unfrozen surface, the flat surface will still enhance the return and could lead to a strong peak in the waveform. Figure 13 illustrates some strong signals in the middle of the waveforms of a 50 km section of the 7 August 2011 ascending pass over the test area in west Greenland. These may originate from extended surfaces orthogonal, or nearly orthogonal, to the incident wave. We have selected one such strong signal, labelled as 'L1' in Fig. 13, which is detected in results from ascending and descending passes from all the summers from 2010 to 2016. The supplementary material contains a sequence of 14 summer MODIS images from 2012 to 2016 which show that the L1 and L2 features are above the snow line for all 5 years and that the surface of these depressions did not become totally ice free. Figure 14 shows the positions of the sub-satellite tracks superimposed on a summer 2016 Landsat 8 image, and that there were dark regions, presumably wet snow, at the positions of the topographic lows marked as L1 and L2. The relative strength of the CryoSat return signals for the seven ascending passes for both features are shown in Fig. 15 and the year-to-year derived height in Fig. 16 with details provided in Table 1. The sequence of dates for the repeat ascending passes are Aug. 4, 2010; Aug. 7, 2011; Aug. 9, 2012; Aug. 12, 2013; Aug 16, 2014; Aug. 19, 2015, and Aug. 21, 2016 reflecting the 369.25-day repeat orbit cycle. The repeat descending passes are 5.5 days after the ascending passes.

Our interpretation of the strengths of the lake signatures and the surface elevation is as follows: Considering the low surface velocity (~ 3.5 m/year, Joughin et al., 2012, 2016), and elevation (~1600 m) at this position, it is unlikely that either of these depressions drained in the manner of the lakes in the ablation zone in any of the summers. The increase in height from the

summer 2010 to 2012 (Fig. 16) may reflect the melt at these positions, which was particularly strong in 2012 (see e.g. Fettweis, http://climato.be/melt-2016). However, the decrease in elevation in subsequent years is then a problem. The discovery that water can persist for years in firn aquifers (Koenig et al., 2014, Forster et al., 2014), suggests that the decrease in elevation after 2012 may reflect a slow percolation of the meltwater into the firn. Clearly, the specific causes of the decrease in elevation of L1 and L2 after 2012, and the difference between the L1 and L2 height change, are not known.

The Landsat 8 image from July 6 2016 (Fig. 17) includes one 2.4 x 1 km lake at 70.37 N, 49.79 W, and ~1020 m in elevation, which was detected in the CryoSat waveforms from all the ascending and descending repeat passes listed on Fig. 17 between 2011 and 2016. By the time of the Landsat 8 image in 2016 most of the snow had melted and we surmise that melt had been on-going during June and early July for the years 2011 – 2016 at this position, and at the times of the CryoSat over-passes (Fig. 17 and Table 2). Figure 18 illustrates the lake height for all passes except for the 2013 descending pass which was too far to the west of the lake for reliable results. In contrast to the high elevation, low melt 'lake' described above, now there is a clear height increase in the 5.5 days between the ascending and descending passes over the lake. This allows an estimate of the filling rate at the time of the two passes. If we assume a lake area of 2 ± 0.5 km^2 this implies a filling rate of ~$0.2. 10^6 – 2.10^6$ m^3 melt water added per day. This lake does drain sometime after the start of July, see the MODIS sequence in the supplementary material, but appears not to have drained at the times of any of the CryoSat overpasses.

5 Discussion

In this section we discuss the two SARIn processing approaches and the limitations and successes of the current CryoSat SARIn products for glacial ice.

There are two important advantages with swath processing: firstly, there is no need for a retracker and, secondly, the swath data is obtained predominantly from the region directly beneath the satellite and the look angles for the swath footprints can be less than those for the POCA (for those areas with cross-track slopes appropriate for swath processing). With the small look angles, the footprint illumination cross-track is essentially uniform. Consequently, assuming a small contribution from the range ambiguous area, the phase should represent the geometric centre of the footprint so that the range, satellite state vectors, and the various angles should lead to reliable heights. Unfortunately, the roll-angle problem discussed earlier compromises the swath mode results as the resulting cross-track mis-mapping will normally lead to a height error (Gray et al., 2013).

POCA processing requires a retracker and the look angle can extend into the range in which the illumination cross-track is affected by the antenna pattern variation so that the phase may not reflect the geometric centre of the footprint. Rather it may be displaced towards the sub-satellite track. With interferometric swath processing, precise knowledge of the baseline and baseline angles is important (Rosen et al. 2000), and with the CryoSat roll-angle problem individual POCA heights are

normally more precise than swath mode heights. For height change estimates, however, both POCA and swath mode results can be combined as long as any bias is accounted for. Foresta et al. (2016) used primarily swath mode results in a study of elevation change of Icelandic ice caps, showing the improved surface coverage of swath mode, and that height change information could be derived from these results. Also, Smith et al. (2016) combined swath and POCA data to document surface height change on the Thwaites Glacier. But in this case 'meter scale biases', correlated over tens of kilometres but independent orbit-to-orbit, were partially corrected by combining with the POCA data.

The known problem in processing the star-tracker data (Scagliola et al., 2017), and the resulting varying error in the reported value of the baseline roll angle, can have an impact on the precision of the CryoSat height results. Any roll-angle error translates directly into a cross-track mapping error so that the resulting height error then depends on the angle between the incident wave and the tangent to the cross-track surface. If this angle is 90° and the surface slope changes slowly over a few hundred meters, then the error is small as the geocoding algorithm produces the correct elevation for the mis-mapped footprint. Although we show that the roll-angle problem had essentially no impact on the Devon POCA results, it did have an impact on the POCA results from the west Greenland test site. In this case the cross-track slopes varied more rapidly than for Devon and lead to the situation where an incorrect roll angle could lead to an increase in the CryoSat height with respect to the surface irrespective of the sense of the roll-angle error. This we suggest is the origin of the unrealistic result that the average POCA height was slightly above the physical surface for the west Greenland site.

POCA heights originate from ridges and peaks and, when the cross-track slope is appropriate for swath processing, the swath mode results will normally originate from the area beneath the satellite so the two approaches are complementary in surface coverage. As discussed above, there can be a bias between POCA and swath heights which needs to be considered if the results are merged. The potential height error for individual estimates is normally less for POCA data than for swath mode heights but the exception is the precision with which one can estimate the height of relatively large supraglacial lakes when the lake is beneath the satellite and viewed at close to normal incidence. In this case, we have a very strong signal in the middle of the waveform, any range ambiguous contribution should be small, and no retracker is required for the geocoding solution. Further, with this viewing geometry the problem of an incorrect roll angle leads to a small error in the lake surface height and a precision of ~ 0.5 m is possible for the surface height of a large lake. Work is underway to better evaluate the extent to which CryoSat data can help in quantifying the time and extent of melt around Greenland.

The ability to geocode the relatively small footprint possible with the SARIn mode over glacial ice creates a huge advantage for this mode over the traditional low resolution radar altimetry. Future radar altimeters employing coherent along-track processing, either fully focussed or Delay-Doppler, coupled with cross-track interferometry, could play a very important role in monitoring change on many ice caps and glaciers.

6 Conclusions

Here we list the specific conclusions arising from our analysis of the SARIn data over Devon Ice Cap and west Greenland.

1. A more consistent fit can be obtained between CryoSat and surface heights using the prelaunch baseline coupled with an additional roll-angle bias of ~ 0.0075°. Although the additional bias may originate with the angle measurement, it could equally well be an equivalent, additional phase correction of ~0.0435 radians to the value of 0.612 radians currently used in the baseline C product (Bouzinac, 2012).

2. A retracker which uses the first significant leading edge of the waveform normally leads to more reliable elevations than a retracker that uses the whole waveform, this appears to be particularly true for areas like West Greenland in which the shape of the waveform is very variable and the peak signal is often in the middle of the waveform.

3. Swath mode results complement the POCA results but are normally less precise. The exception is the precision with which the heights of supraglacial lakes can be obtained when the satellite flies almost directly over the lake.

4. The uncertainty in the CryoSat baseline roll angle affects primarily swath mode results but can also impact the precision of POCA results when the surface topography is comparable to that in the west Greenland test site.

5. While more work is required to establish to what extent CryoSat SARIn waveforms and heights can improve our knowledge of melt in the ablation zone of the Greenland Ice Sheet, these initial results are encouraging that CryoSat SARIn data can help provide useful information on the variation of year-to-year melt.

Acknowledgements

This work was supported by the European Space Agency through the provision of CryoSat-2 data and the support for the CRYOVEX airborne field campaigns in both the Canadian Arctic and Greenland. NASA supported the IceBridge flights over the Canadian Arctic and Greenland, while NSIDC facilitated provision of the airborne laser data. The Technical University of Denmark (TUD) managed the ESA supported flights over Devon. The IceBridge and TUD teams are gratefully acknowledged for the acquisition and provision of the airborne data used in this work. The Polar Continental Shelf Project (Natural Resources Canada) provided logistic support for field work in the Canadian Arctic, and the Nunavut Research Institute and the community of Resolute Bay gave permission to conduct research on the Devon Ice Cap. Support for D. Burgess was provided through the Climate Change Geoscience Program, Earth Sciences Sector, Natural Resources Canada and the GRIP programme of the Canadian Space Agency. Support for K. Langley was provided by ESA project Glaciers-CCI (4000109873/14/I-NB). T. Dunse and G. Moholdt were supported by ESA-Prodex project 4000 110 725/724 "CRYOVEX" and T. Dunse was supported by the Nordforsk-funded project Green Growth Based on Marine Resources: Ecological and Sociological Economic Constraints (GreenMAR). Wesley Van Wychen and Tyler de Jong helped with the 2011 kinematic GPS survey on Devon. NSERC funding to L. Copland is gratefully acknowledged. We also acknowledge NASA and NSIDC for the provision of the Landsat 8 and MODIS imagery.

Tommaso Parrinello, ESA, and Michele Scagliola, Aresys, provided information on the problem in processing the star-tracker data. We also appreciate the work of the editor, Dr. Ian Howat, and the three anonymous reviewers who provided thoughtful and helpful reviews.

References

Bamber, J. L.: Ice sheet altimeter processing scheme, Int. J. Remote Sens., 15, 925–938, doi:10.1080/01431169408954125, 1994.

5   Bouzinac, C.: CryoSat-2 Product Handbook, Tech. Report, European Space Agency, available at: http://emits.sso.esa.int/emits-doc/ESRIN/7158/CryoSat-PHB-17apr2012.pdf (last access: 9 July 2016).

Brenner, A. C., Bindschadler, R. A., Thomas, R. H., and Zwally, H. J.: Slope-induced errors in radar altimetry over continental ice sheets, J. Geophys. Res., 88, 1617–1623, 1983.

10   Brenner, A. C., DiMarzio, J. P., and Zwally, H. J.: Precision and accuracy of satellite radar and laser altimeter data over the continental ice sheets, IEEE T. Geosci. Remote. Sens., 45, 321–331, doi:10.1109/TGRS.2006.887172, 2007.

Buffard, J.: CryoSat-2 Level 2 product evolutions and quality improvements in Baseline C, ESA technical report XCRY-15   GSEG-EOPG-TN-15-00004. Available from https://earth.esa.int/web/guest/document-library, 2015.

Christie, F. D. W., Bingham R. G., Gourmelen N., Tett S. F. B., and Muto A.: Four-decade record of pervasive grounding line retreat along the Bellingshausen margin of West Antarctica, Geophys. Res. Lett., 43, 5741–5749, doi:10.1002/2016GL068972, 2016.

20   Davis, C. H.: A robust threshold retracking algorithm for measuring ice-sheet surface elevation change from satellite radar altimeters, IEEE T. Geosci. Remote, 35, 974–979, doi:10.1109/36.602540, 1997.

Davis, C. H. and Ferguson, A. C.: Elevation change of the Antarctic ice sheet, 1995-2000, from ERS-2 satellite radar 25   altimetry, IEEE Trans. Geosci. Remote Sens., 42(11), 2437–2445, doi:10.1109/TGRS.2004.836789, 2004.

Echelmeyer, K., T.S. Clarke and W.D. Harrison.: Surficial glaciology of Jakobshavns Isbræ, West Greenland: Part I. Surface morphology. J. Glaciol., 37(127), 368–382, 1991.

30   Fitzpatrick, A. A. W., Hubbard, A. L., Box, J. E., Quincey, D. J., van As, D., Mikkelsen, A. P. B., Jones, G. A.: A decade (2002-2012) of supraglacial lake volume estimates across Russell Glacier, West Greenland. The Cryosphere, 8(1), 107-121. doi: 10.5194/tc-8-107-2014, 2014.

Foresta, L, Gourmelen, N, Pálsson, F, Nienow, P, Björnsson, H and Shepherd, A.: Surface Elevation Change and Mass 35   Balance of Icelandic Ice Caps Derived from Swath Mode CryoSat-2 Altimetry, Geophys. Res. Lett., 43, 12138–12145, doi:10.1002/2016GL071485, 2016.

Forster, R. R., Box, J. E., van der Broeke, M. R., Miege, C., Burgess, E. W., van Angelen, J. H., Lenaerts, J. T. M., Koenig, L. S., Paden, J, Lewis, C., Gogenini, S. P., Leuschen, C., and McConnell, J. R.: Extensive liquid meltwater storage in firn 40   within the Greenland ice sheet, Nature Geosc., 7, 95-98, doi:10.1038/ngeo2043, 2014.

Galin, N., Wingham, D. J., Cullen, R., Fornari, M., Smith, W. H. F., and Abdall, S.: Calibration of the CryoSat-2 Interferometer and Measurement of Across-track Ocean Slope, IEEE T. Geosci. Remote., 51, 57–72, 2012.

45   Gray, L., Burgess, D., Copland, L., Cullen, R., Galin, N., Hawley, R. and Helm, V.: Interferometric swath processing of Cryosat data for glacial ice topography, the Cryosphere, 7(6), 1857–1867, doi:10.5194/tc-7-1857-2013, 2013.

Gray, L., Burgess, D., Copland, L., Demuth, M. N., Dunse, T., Langley, K. and Schuler, T. V.: CryoSat-2 delivers monthly and inter-annual surface elevation change for Arctic ice caps, The Cryosphere, 9(5), 1895–1913, doi:10.5194/tc-9-1895-2015, 2015.

5   Gray L., Burgess, D., Copland L., Dunse, T., Hagen, J.O., Langley, K., Moholdt, G., Schuler, T., and Van Wychen, W.: On the bias between ice cap surface elevation and Cryosat results. Proc. 'Living Planet Symposium 2016', Prague, Czech Republic, 9–13 May 2016, ESA SP-740, August 2016.

Hawley, R.L., Shepherd, A., Cullen, R., & Wingham, D.J.: Ice-sheet elevations from across-track processing of airborne
10 interferometric radar altimetry. Geophys. Res. Lett., 36, L25501, doi:10.1029/2009GL040416, 2009.

Helm, V., Humbert, A., and Miller, H.: Elevation and elevation change of Greenland and Antarctica derived from CryoSat-2, The Cryosphere, 8, 1539–1559, doi:10.5194/tc-8-1539-2014, 2014.

15 Howat, I. M., Negrete, A. and Smith, B. E.: The Greenland Ice Mapping Project (GIMP) land classification and surface elevation data sets, The Cryosphere, 8(4), 1509–1518, doi:10.5194/tc-8-1509-2014, 2014.

Hurkmanns, R. T. W. L., Bamber, J. L., and Griggs, J. A.: Importance of slope-induced error correction in volume change estimates from radar altimetry, The Cryosphere, 6, 447–451, doi:10.5194/tc-6-447-2012, 2012.
20
Hurkmanns, R. T. W. L., Bamber, J. L., Davis, C. H., Joughin, I. R., Khvorostovsky, K. S., Smith, B. S. and Schoen, N.: Time-evolving mass loss of the Greenland Ice Sheet from satellite altimetry, The Cryosphere, 8, 1725–1740, doi:10.5194/tc-8-1725-2014, 2014.

25 Ignéczi, Á., Sole A. J., Livingstone S. J., Leeson A. A., Fettweis X., Selmes N., Gourmelen N., and Briggs, K.: Northeast sector of the Greenland Ice Sheet to undergo the greatest inland expansion of supraglacial lakes during the 21st century, Geophys. Res. Lett., 43, 9729–9738, doi:10.1002/2016GL070338, 2016.

Jensen, J. R.: Angle measurement with a phase monopulse radar altimeter, IEEE T. Antenn. Propag., 47, 715–724, 1999.
30
Joughin, I., Howat, I. M., Fahnestock, M., Smith, B., Krabill, W., Alley, R. B., Stern, H., and Truffer, M.: Continued evolution of Jakobshavn Isbræ following its rapid speedup, J. Geophys. Res., 113, F04006, doi:10.1029/2008JF001023, 2008.

35 Joughin, I., Smith, B. E., Howat, I., and Scambos, T.: MEaSUREs Multi-year Greenland Ice Sheet Velocity Mosaic, Version 1. Boulder, Colorado USA. NASA National Snow and Ice Data Center Distributed Active Archive Center. doi: http://dx.doi.org/10.5067/QUA5Q9SVMSJG [accessed 9/6/2016]. 2016.

Joughin, I., Smith, B. E., Howat, I., Scambos, T. and Moon, T.: Greenland Flow Variability from Ice-Sheet-Wide Velocity
40 Mapping, Journal of Glaciology. 56. 415-430. http://dx.doi.org/10.3189/002214310792447734, 2010.

Kleinherenbrink, M., Ditmar, P.G., Lindenbergh, R.C.: Retracking Cryosat data in the SARIn mode and robust lake level extraction. Rem. Sens. Env., 152, 38-50, doi.org/10.1016/j.rse.2014.05.014, 2014.

45 Koenig, L. S., Miege, C., Forster, R. R., and Brucker, l.: Initial in situ measurements of perennial meltwater storage in the Greenland firn acquifer, Geophys. Res. Lett., 41, 81-85, doi:10.1002/2013GL058083, 2014.

Krabill, W. B., Abdalati, W., Frederick, E. B., Manizade, S. S., Martin, C. F., Sonntag, J. G., Swift, R. N., Thomas, R. H., and Yungel, J. G.: Aircraft laser altimetry measurement of elevation changes of the Greenland ice sheet: technique and
50 accuracy assessment, J. Geodyn., 34, 357–376, 2002.

Krabill, W. B.: IceBridge ATM L2 Icessn Elevation, Slope, and Roughness, Version 2. [ILATM2.002]. Boulder, Colorado USA. NASA National Snow and Ice Data Center Distributed Active Archive Center. doi: http://dx.doi.org/10.5067/CPRXXK3F39RV. [Accessed 31/10/2016], 2014, updated 2016.

Leeson, A. A., Shepherd, A., Briggs, K., Howat, I., Fettweis, X., Morlighem, M., and Rignot, E.: Supraglacial lakes on the Greenland ice sheet advance inland under warming climate, Nature Climate Change, 5, 51-55, doi:10.1038/nclimate2463, 2015.

10   Levinsen, J. F., Simonsen, S. B., Sorensen, L. S., Forsberg, R.: The Impact of DEM Resolution on relocating Radar Altimetry Data over Ice Sheets, IEEE J Sel. Topics in Appl. Earth Obs. and Rem. Sens., 9, 3158-3163, doi: 10.1109/JSTARS.2016.2587684, 2016.

Liang, Y. L., Colgan, W., Lv, Q., Steffen, K., Abdalati, W., Stroeve, J., Gallaher, D., and Bayou, N.: A decadal investigation
15   of supraglacial lakes in West Greenland using a fully automatic detection and tracking algorithm, Remote Sens. Environ., 123, 127–138, 2012.

McMillan, M., Nienow, P., Shepherd, A., Benham, T. and Sole, A.: Seasonal evolution of supraglacial lakes on Greenland Ice Sheet. Earth Planetary Sc. Ltrs, 262, 484-492, 2007.

20   Nghiem, S. V., Steffen, K., Kwok, R., and Tsai, W.-Y.: Detection of snowmelt regions on the Greenland ice sheet using diurnal backscatter change, J. Glaciol., 47(159), 539-547, doi: https://doi.org/10.3189/172756501781831738, 2001.

Nilsson, J., Vallelonga, P., Simonsen, S. B., Sørensen, L. S., Forsberg, R., Dahl-Jensen, D., Hirabayashi, M., Goto-Azuma, K., Hvidberg, C. S., Kjaer, H. A. and Satow, K.: Greenland 2012 melt event effects on CryoSat-2 radar altimetry, Geophys. Res. Lett., 42(10), 3919–3926, doi:10.1002/2015GL063296, 2015.

Nilsson, J., Gardner, A., Sandberg Sorensen, L., and Forsberg, R.: Improved retrieval of land ice topography from CryoSat-2 data and its impact for volume change estimation of the Greenland Ice Sheet, The Cryosphere Discuss., doi:10.5194/tc-2016-109, accepted, 2016.

30   Qi, W. and Braun, A.: Accelerated Elevation Change of Greenland's Jakobshavn Glacier Observed by ICESat and IceBridge, IEEE GRS Letters, 10, 1133-1137, doi:10.1109/ LGRS.2012.2231954, 2013.

Raney, R. K.: The delay/Doppler radar altimeter, IEEE T. Geosci. Remote, 36, 1578–1588, 1998.

35   Remy, F., Parouty, S.: Antarctic Ice Sheet and Radar Altimetry: A Review. Remote Sens., 4, 1212-1239, doi:10.3390/rs1041212, 2009.

Rosen, P., Hensley, S., Joughin, I., Li, F., Madsen, S., Rodriguez, E., and Goldstein, R.: Synthetic Aperture Radar Interferometry, Proc. IEEE, 88, 333–382, 2000.

Scagliola, M, Fornari, M., Bouffard, J. and Parrinello, T.: The CryoSat interferometer: end-to-end calibration and achievable performance, submitted for publication in Adv. In Space Res., 2017.

Shepherd, A., Ivins, E. R., A., G., Barletta, V. R., Bentley, M. J., Bettadpur, S., Briggs, K. H., Bromwich, D. H., Forsberg,
45   R., Galin, N., Horwath, M., Jacobs, S., Joughin, I., King, M. A., Lenaerts, J. T. M., Li, J., Ligtenberg, S. R. M., Luckman, A., Luthcke, S. B., McMillan, M., Meister, R., Milne, G., Mouginot, J., Muir, A., Nicolas, J. P., Paden, J., Payne, A. J., Pritchard, H., Rignot, E., Rott, H., Sandberg Sørensen, L., Scambos, T. A., Scheuchl, B., Schrama, E. J. O., Smith, B., Sundal, A. V., van Angelen, J. H., van de Berg, W. J., van den Broeke, M. R., Vaughan, D. G., Velicogna, I., Wahr, J. D.,

Whitehouse, P. L., Wingham, D. J., Yi, D., Young, D., and Zwally, H. J.: A Reconciled Estimate of Ice-Sheet Mass Balance, Science, 338, 1183–1189, doi:10.1126/science.1228102, 2012.

Sneed, W. and Hamilton, G.: Evolution of melt pond volume of the surface of the Greenland Ice Sheet, Geophys. Res. Lett., 34, L03501, doi:10.1029/2006GL028697, 2007.

Smith, B. E., Gourmelen, N., Huth, A., and Joughin, I.: Connected subglacial lake drainage beneath Thwaites Glacier, West Antarctica, The Cryosphere Discuss., doi:10.5194/tc-2016-180, in review, 2016.

Ulaby, F., Moore, R., and Fung, A.: Microwave Remote Sensing: Active and Passive, Vol. 2, Norwood, Massachusetts, Artech House, 816–920, 1986.

Wang, L., Toose, P., Brown, R. and Derksen, C.: Frequency and distribution of winter melt events from passive microwave satellite data in the pan-Arctic, 1998-2013, The Cryosphere, 10, 2589–2602, doi:10.5194/tc-10-2589-2016, 2016.

Wingham, D., Francis, C. R., Baker, S., Bouzinac, C., Cullen, R., de Chateau-Thierry, P., Laxon, S. W., Mallow, U., Mavrocordatos, C., Phalippou, L., Ratier, G., Rey, L., Rostan, F., Viau, P., and Wallis, D.: CryoSat-2: a mission to determine the fluctuations in earth's land and marine ice fields, Adv. Space Res., 37, 841–871, 2006.

Zwally, H. J., Li, J., Robbins, J. W., Saba, J. L., Yi, D., Brenner, A. C.: Mass gains of the Antarctic ice sheet exceed losses, J. Glaciol., 61, 1019-1036, doi: 10.3189/2015JoG15J071, 2015.

Year L1	Date	Pass direction	Local time	Min dB	Standard deviation, m (no. of samples)	Look angle (deg.)	Height (m)	Height error (estimated, ± m)
2010	Aug 4	Ascending	1:03	-130	0.52 (61)	0.08±0.006°	1606.5	0.5
	Aug 9	Descending	13:33	-135	0.58 (61)	-0.18±0.006°	1606.3	0.6
2011	Aug 7	Ascending	6:48	-130	0.48 (51)	-0.05±0.006°	1609.1	0.5
	Aug 12	Descending	19:18	-134	0.41 (57)	-0.22±0.006°	1609.5	0.5
2012	Aug 9	Ascending	12:33	-125	0.63 (52)	-0.05±0.006°	1613.8	0.6
	Aug 15	Descending	1:03	-127	0.29 (59)	-0.2±0.006°	1614.3	0.4
2013	Aug 12	Ascending	18:16	-135	0.59 (73)	-0.1±0.006°	1612.5	0.6
	Aug 18	Descending	6:46	-139	0.33 (48)	-0.2±0.006°	1612.8	0.4
2014	Aug 16	Ascending	0:01	-138	0.56 (75)	0.05±0.006°	1610.8	0.6
	Aug 21	Descending	12:32	-130	0.46 (74)	-0.18±0.006°	1611.2	0.5
2015	Aug 19	Ascending	5:46	-138	0.64 (48)	-0.04±0.006°	1610.2	0.6
	Aug 24	Descending	18:16	-139	0.45 (34)	-0.15±0.006°	1610.3	0.5
2016	Aug. 21	Ascending	11:31	-140	0.49 (34)	-0.02±0.006°	1606.1	0.5
	Aug. 27	Descending	0:01	-140	0.51 (18)	-0.17±0.006°	1606.7	0.6
L2								
2010	Aug 4	Ascending	1:03	-120	0.75 (41)	0.01±0.006°	1571.5	0.7
2011	Aug 7	Ascending	6:48	-134	0.42 (57)	-0.14±0.006°	1573.1	0.5
2012	Aug 9	Ascending	12:33	-130	0.35 (54)	-0.1±0.006°	1576.0	0.4
2013	Aug 12	Ascending	18:16	-135	0.32 (16)	-0.16±0.006°	1573.2	0.5
2014	Aug 15	Ascending	0:01	-135	0.37 (30)	-0.03±0.006°	1572.1	0.4
2015	Aug 19	Ascending	5:46	-137	0.43 (32)	-0.13±0.006°	1572.5	0.5
2016	Aug. 21	Ascending	11:31	-133	0.47 (27)	-0.10±0.006°	1573.1	0.5

Table 1.

Information on the conditions and results of the analysis of the CryoSat data for the two lake features L1 (70.275 N, 48.56 W) and L2 (70.178 N, 48.55 W) shown in Figs 13 and 14. The 'Min dB' column reflects the lower limit of the sample power used in the averaging of the height estimates contained within the window around the surface depression.

Year	Date	Pass direction	Local time	Min dB	SD height (no of samples)	Look angle (deg.)	Height (m)	Height error (estimated ± m)
2011	June 14	ascending	9:33	-125	0.74 (38)	0.03±0.006°	1014.7	0.7
	June 20	descending	22:03	-130	0.59 (41)	-0.07±0.006°	1016.8	0.6
2012	June 16	ascending	15:18	-115	0.77 (56)	0.003±0.006°	1020.4	0.8
	June 22	descending	3:48	-120	0.80 (45)	-0.01±0.006°	1022.3	0.8
2013	June 19	ascending	21:02	-130	0.57 (48)	-0.02±0.006°	1017.1	0.6
	June 25	descending						
2014	June 23	ascending	2:46	-130	0.37 (23)	0.06±0.006°	1018.7	0.4
	June 28	descending	15:16	-135	0.53 (22)	0.03±0.006°	1020.2	0.5
2015	June 26	ascending	8:31	-130	0.67 (39)	-0.001±0.006°	1017.6	0.7
	July 1	descending	21:01	-130	0.87 (29)	-0.07±0.006°	1020.1	0.9
2016	June 28	ascending	14:16	-130	0.74 (62)	0.03±0.006°	1021.4	0.7
	July 4	descending	2;46	-130	0.64 (29)	0.02±0.006°	1022.1	0.6

Table 2.
Information on the conditions and results of the analysis of the CryoSat data for the lake shown in Figs 17 and over-flown by CryoSat on the dates shown.
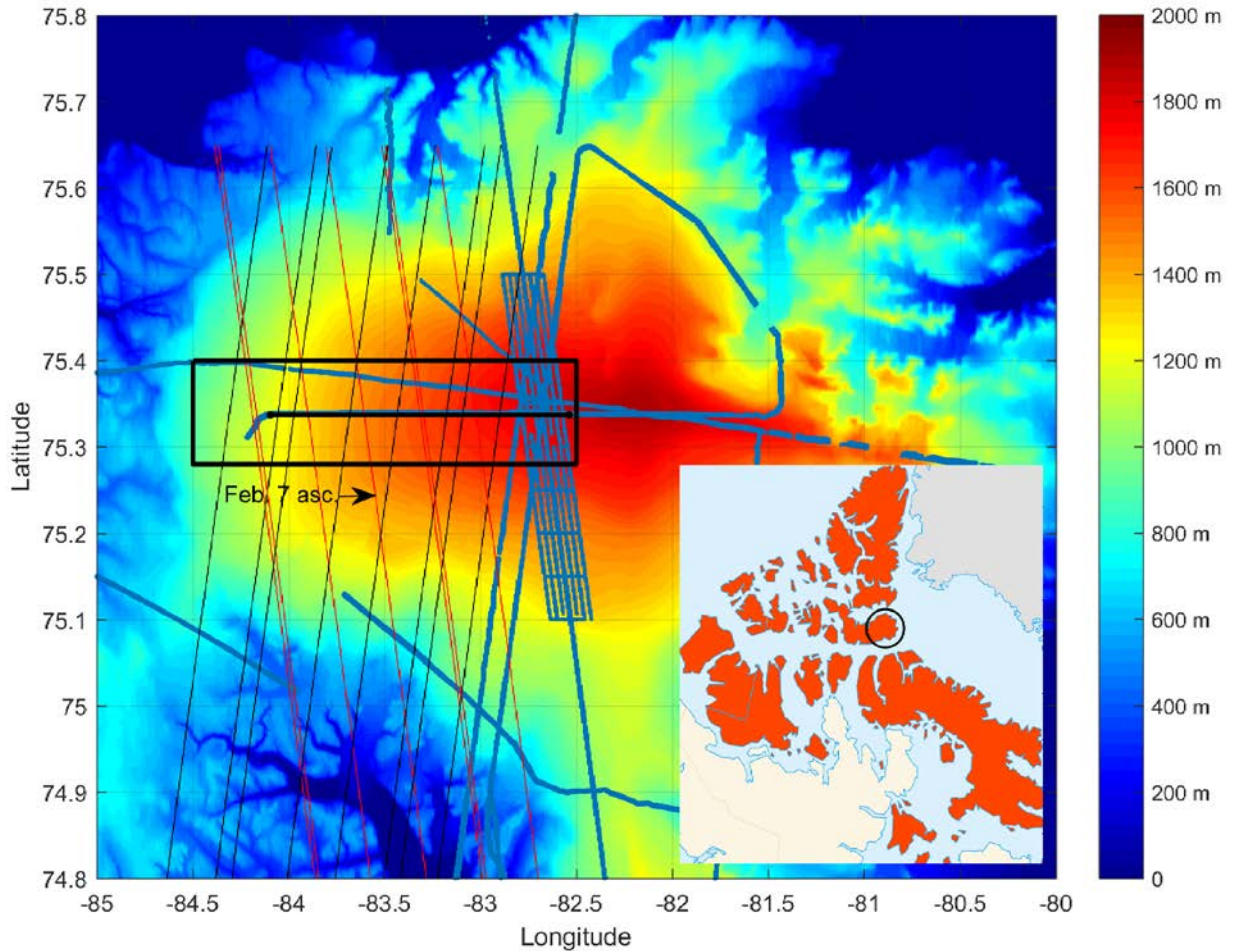
Figure 1: Location of the test area on the western slopes of the Devon Ice Cap (black rectangle). The sub-satellite positions of the spring 2011 ascending and descending passes crossing the test area are shown by the red and black lines respectively. The positions of the reference surface height data are shown in blue, the elevation profile in Fig 3C as a black line, and the sub-satellite track for the waveform power in Fig 6A is labelled. The insert shows the position of Devon Ice Cap (circled) in the Canadian Arctic Archipelago.
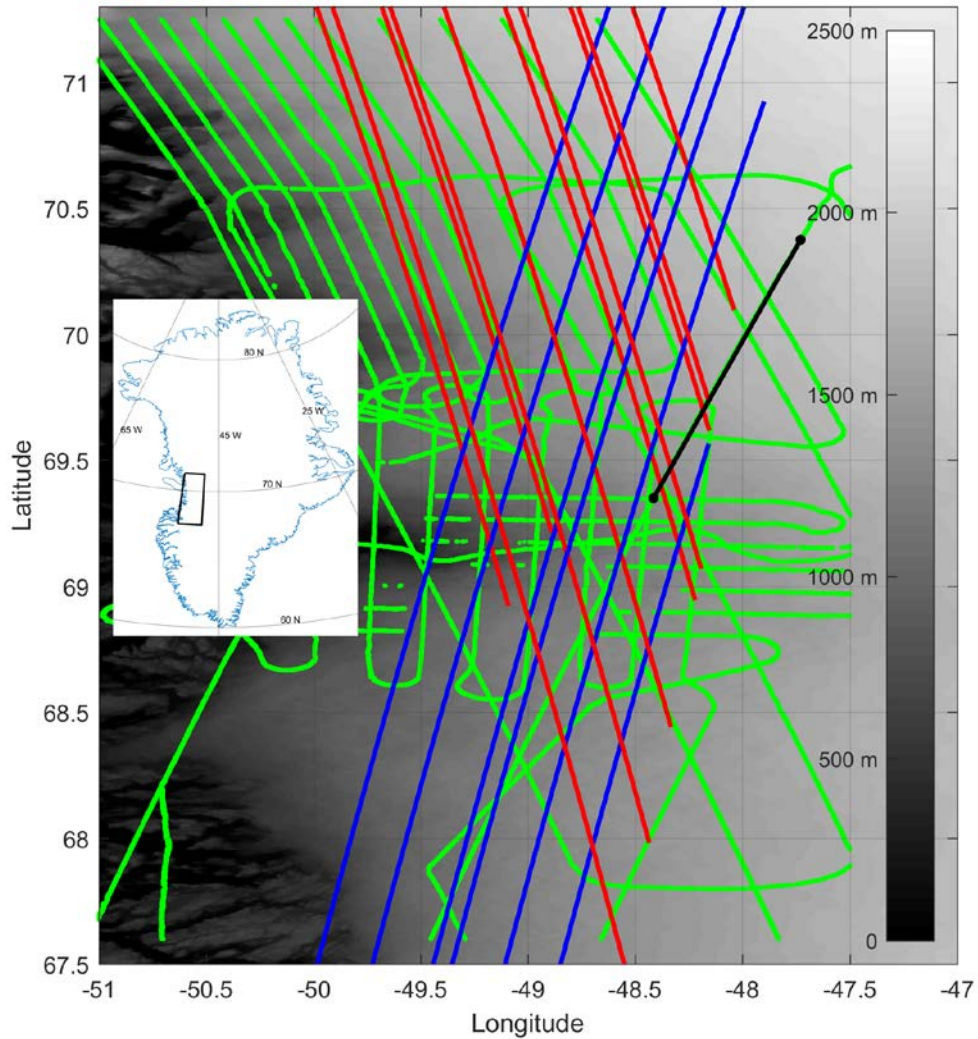
Figure 2: The positions of the reference ATM surface elevations flown by NASA IceBridge missions over the west Greenland site in spring 2011 are shown in green. Sub-satellite CryoSat tracks for the period Jan. 20 to May 16 2011
5 **are shown by red (ascending) and blue (descending) lines. The inset map shows the position of the test area in Greenland and the background image is a black-white representation of the GIMP reference DEM (Howat et al., 2014). The position of the height profile in Fig. 3A is shown by the black line.**
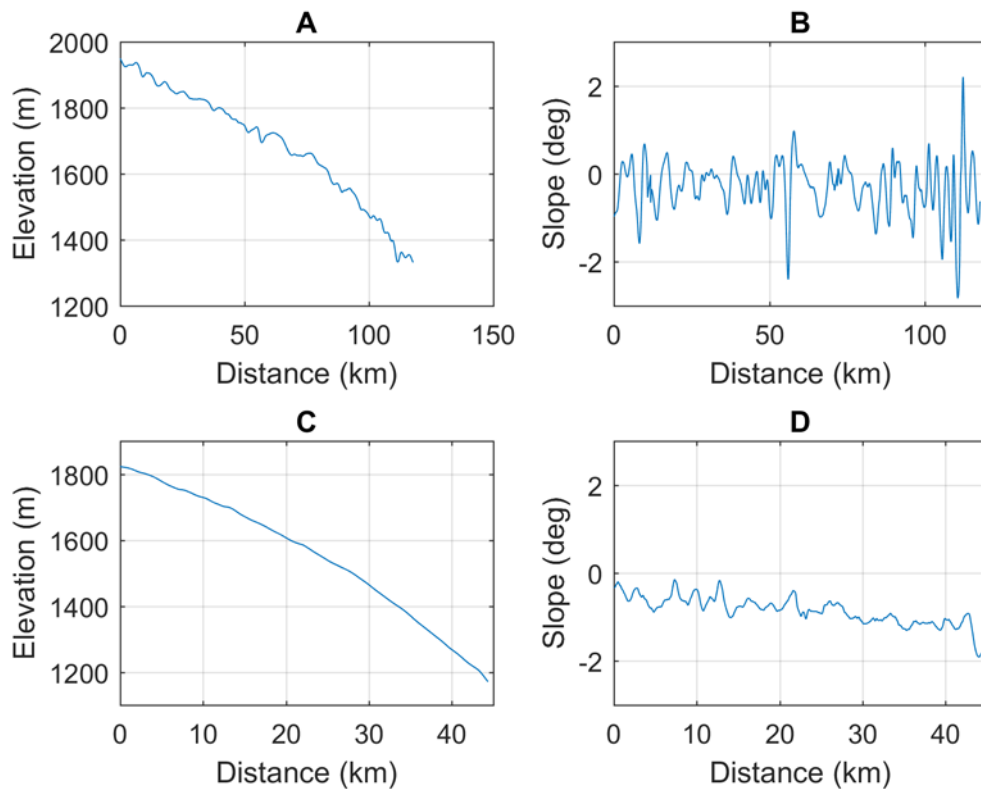
Figure 3: Illustration of the difference in slopes for a typical west Greenland transect (70.37°N, -47.73°W to 69.35°N, -48.42°W, black line in Fig. 2) derived from an ATM flight line from Apr. 6 2011 (box A; elevation and box B; slope) and the EW transect (black line in Fig. 1) from western Devon Ice Cap (box C; elevation and box D slope, Fig. 1).
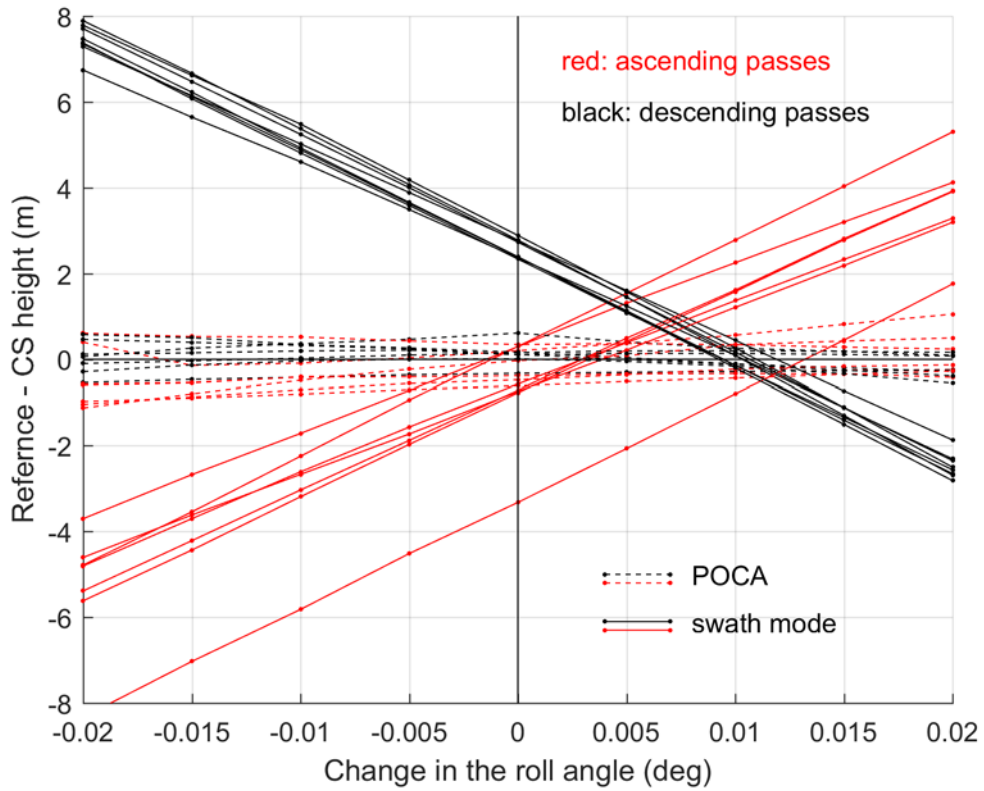
Figure 4: Illustration of the changing bias between the reference and CryoSat (CS) swath mode heights for the Devon test site as an additional roll bias is subtracted from the roll figure given in the L1b file. Results for 7 ascending and 8 descending passes in the winter-spring of 2011 are shown in red and black, respectively. The reference - POCA height variation with the added roll-angle bias is shown with the dashed lines.
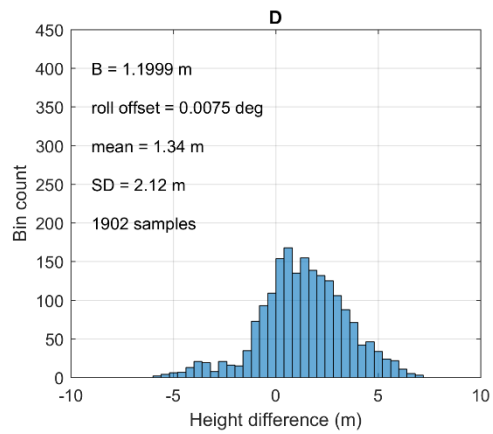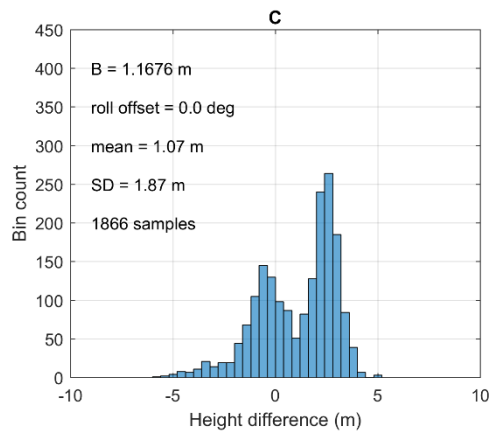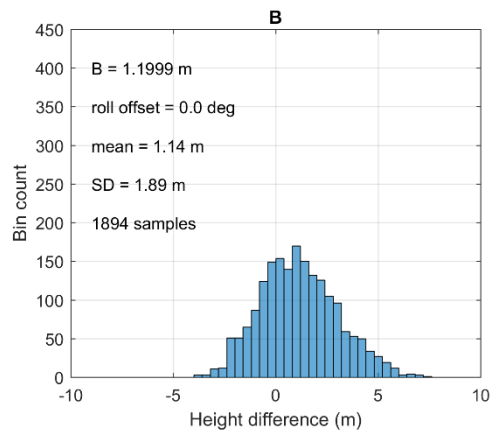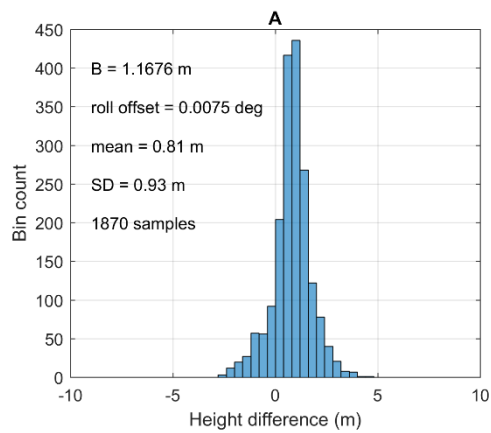
Figure 5: Histograms of the reference minus CryoSat swath heights for Devon Ice Cap: (A) pre-launch baseline and a roll-angle offset of 0.0075°; (B) modified baseline with zero roll offset; (C) pre-launch baseline with zero roll offset; and (D) modified baseline with a roll offset of 0.0075°.
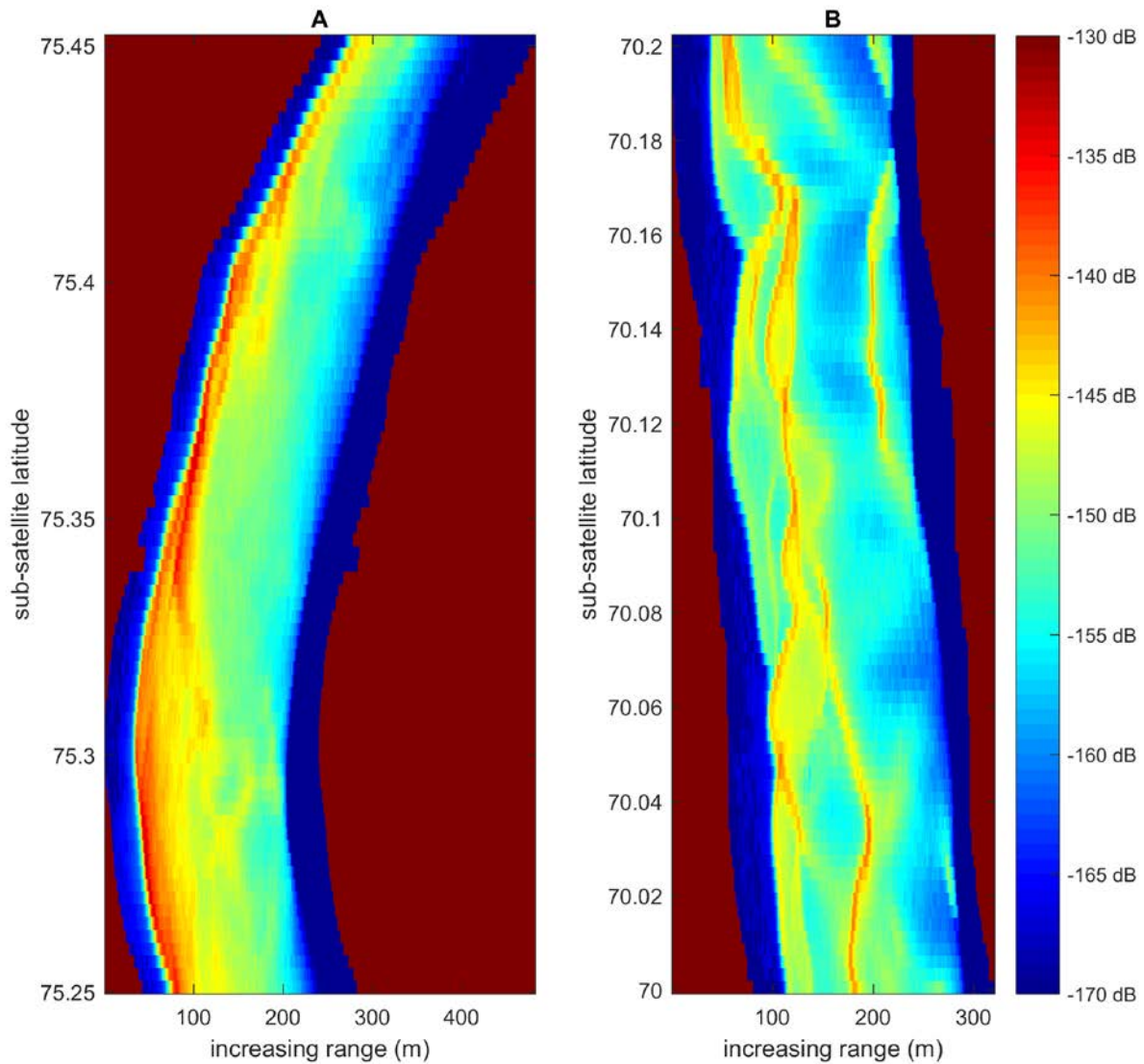
Figure 6. Waveform power for 22 km segments of (A) the Feb. 7 2011 ascending pass over Devon Ice Cap (Fig. 1) and (B) the April 21 2011 descending pass (Fig. 12A) over the west Greenland test site. The return power in dB is represented in colour and the individual waveforms have been shifted in the x direction depending on the time delay to the first sample and the satellite elevation above the WGS84 ellipsoid.
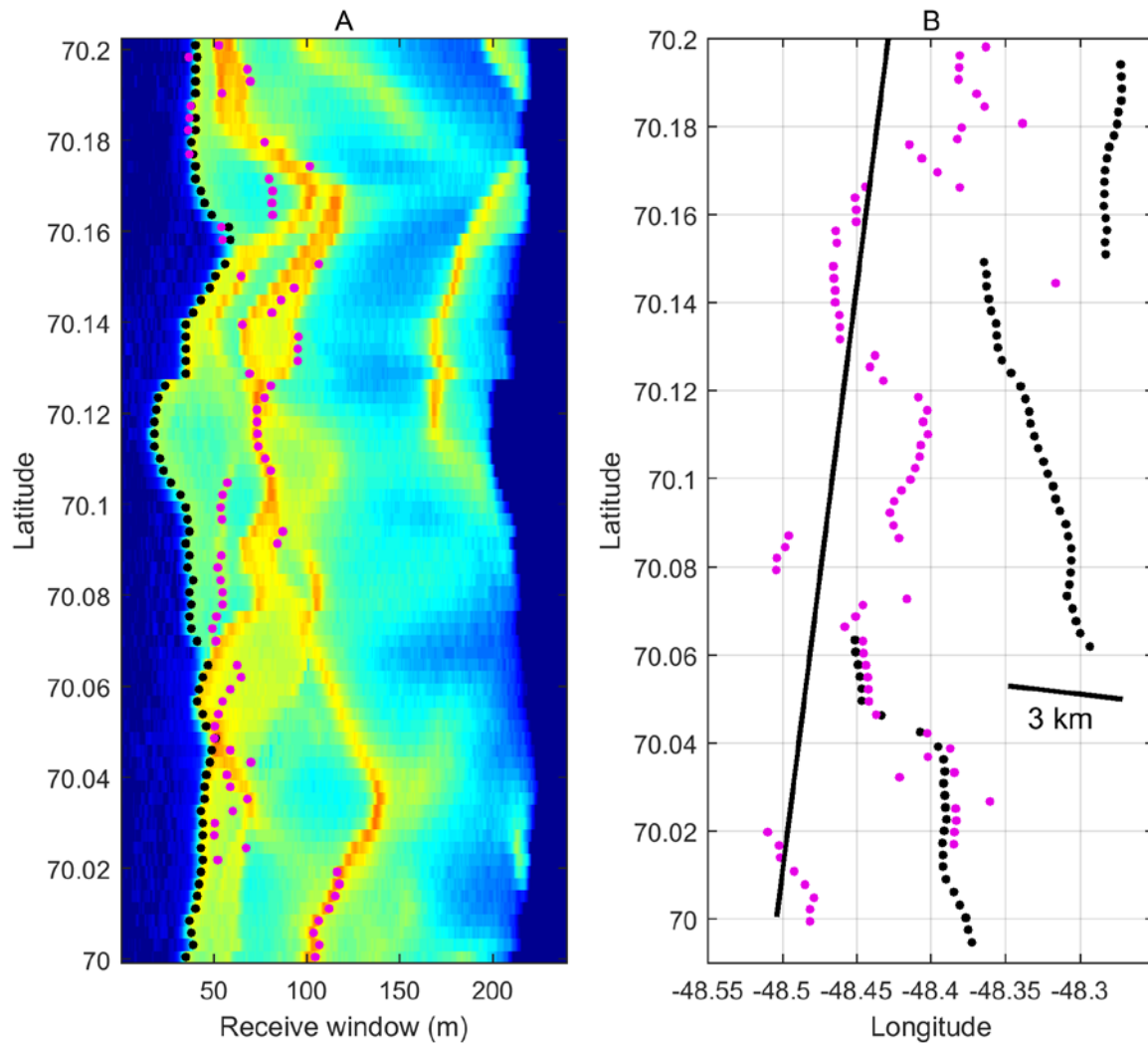
Figure 7. (A) Waveform power without any x axis shifts using the same dB colour scale as in Fig. 6B. The detected POCA positions are shown in (A) for each waveform with black dots, and they clearly correspond to the leading edge of the waveforms. The purple dots are the estimated positions in the waveforms of the L2 POCA solution. **(B)** Geographic positions of the geocoded footprints (black dots) are compared to the positions of the ESA L2 solutions (red dots). The solid black line is the sub-satellite track.
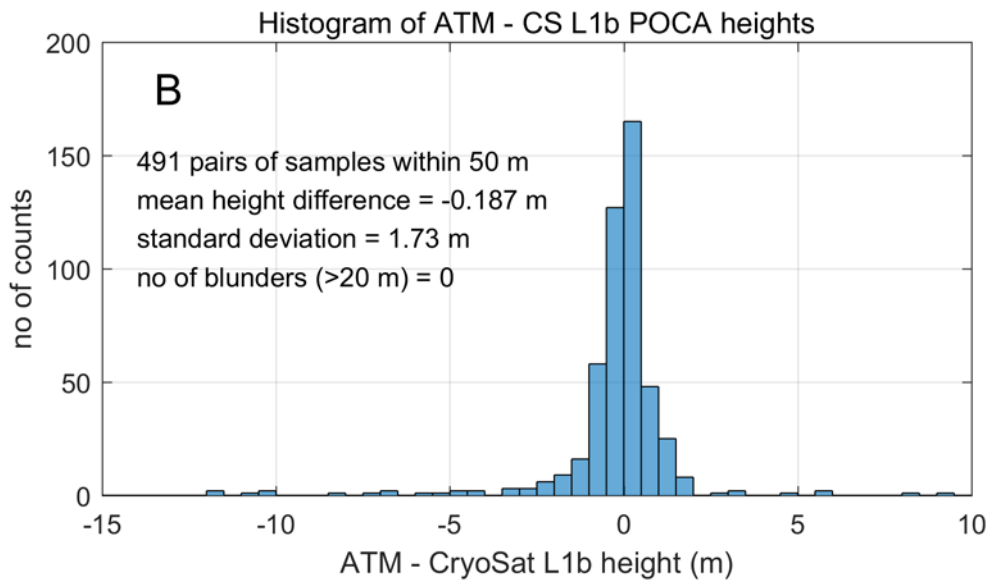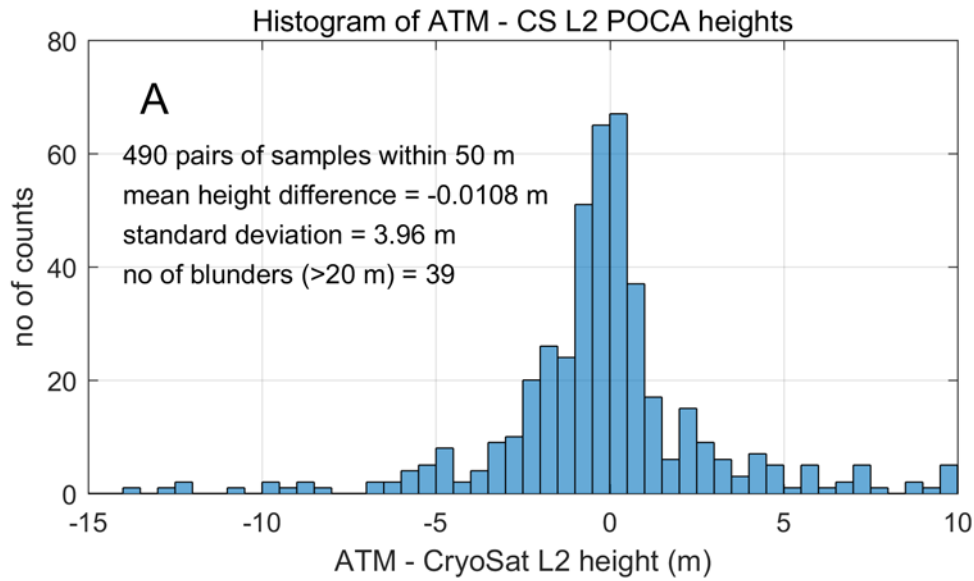
Figure 8. Comparisons of the ATM - CryoSat POCA height difference histograms for the west Greenland test site. (A) the ESA L2 solution: (B) Results from the current maximum slope leading edge retracker. The mean and standard deviation in Fig 8A have been calculated after removal of the 39 blunders. Cryosat data from all the passes between Feb 16 and April 23 2011 have been used in this comparison, and results from the same waveforms used in both cases.
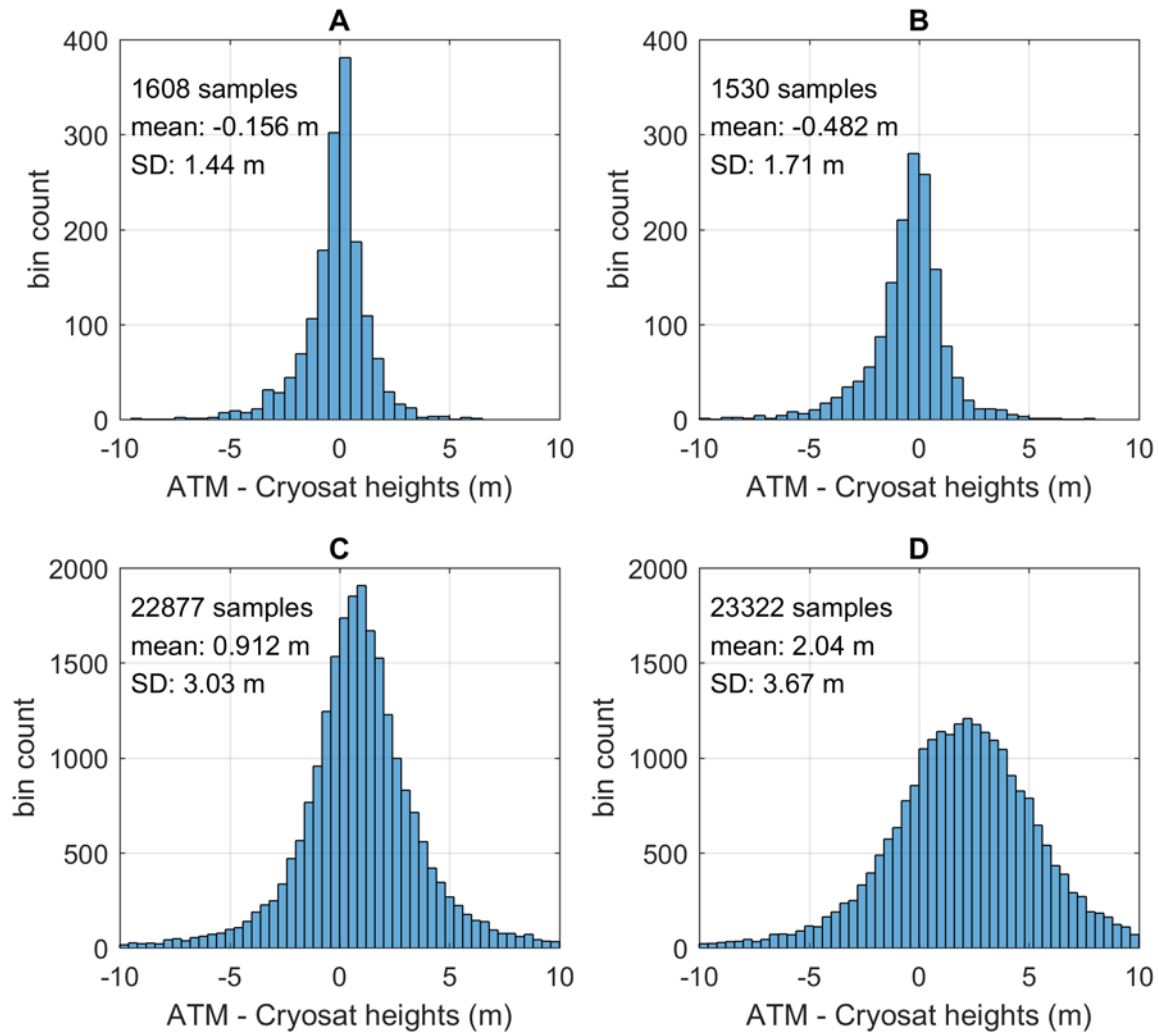
Figure 9. Comparisons of the west Greenland ATM – CryoSat height difference histograms for the solution using the pre-launch baseline coupled with an additional roll offset (A; POCA, C; swath mode solutions). Boxes B and D use the Galin et al. (2013) calibration for the POCA and swath solutions respectively. Results from the CryoSat passes for the period Jan. 20 to May 16 2011 have been used.
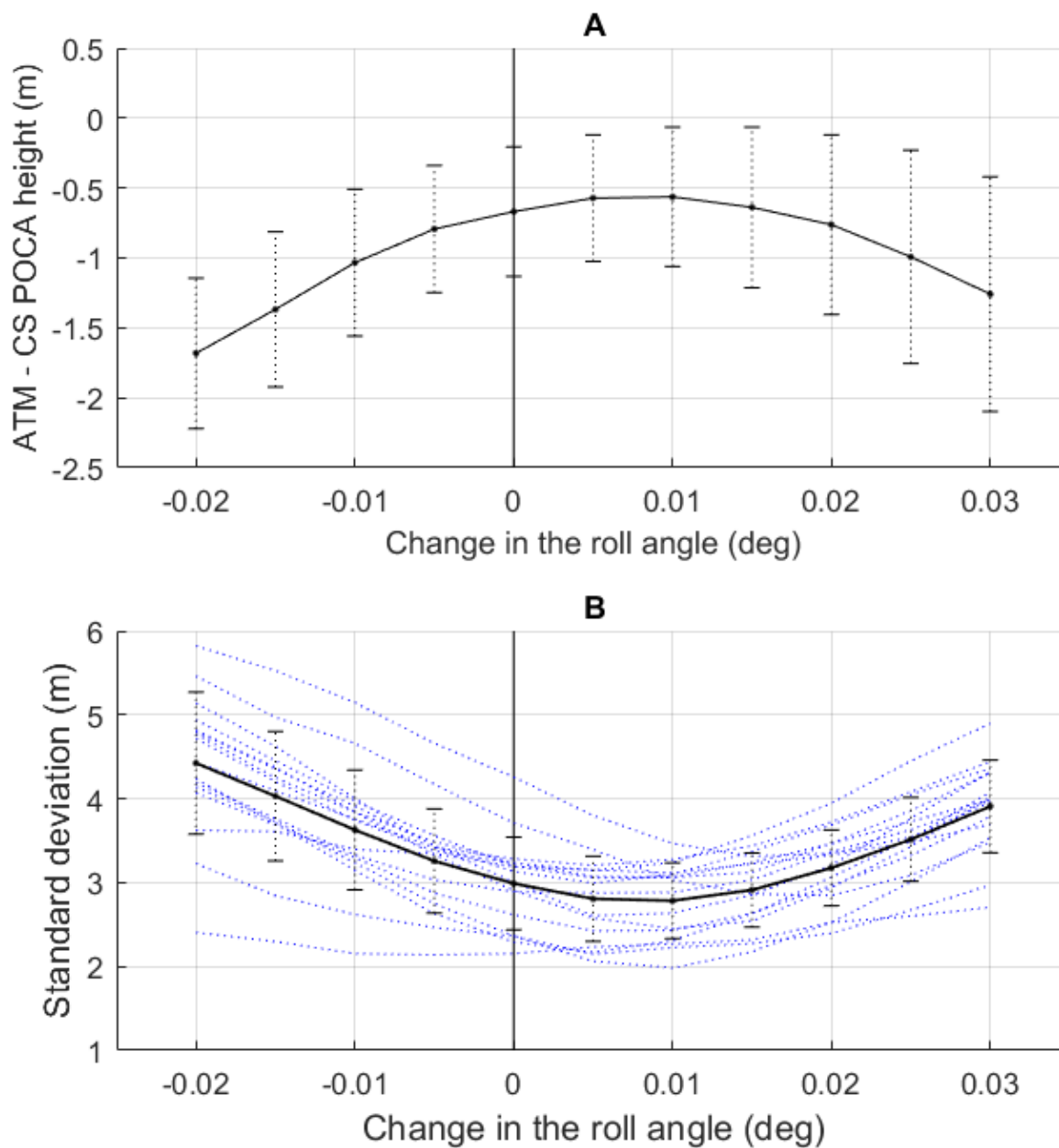
Figure 10. Illustration of the average of the ATM – CryoSat height differences for: (A) 16 passes plotted against the additional roll-angle bias used in the processing. The error bars are ± 1 standard deviation about the mean. (B) Variation in the standard deviation (SD) of the ATM – CryoSat height difference for the individual passes (blue dotted lines) and the average over all the passes (solid black line).
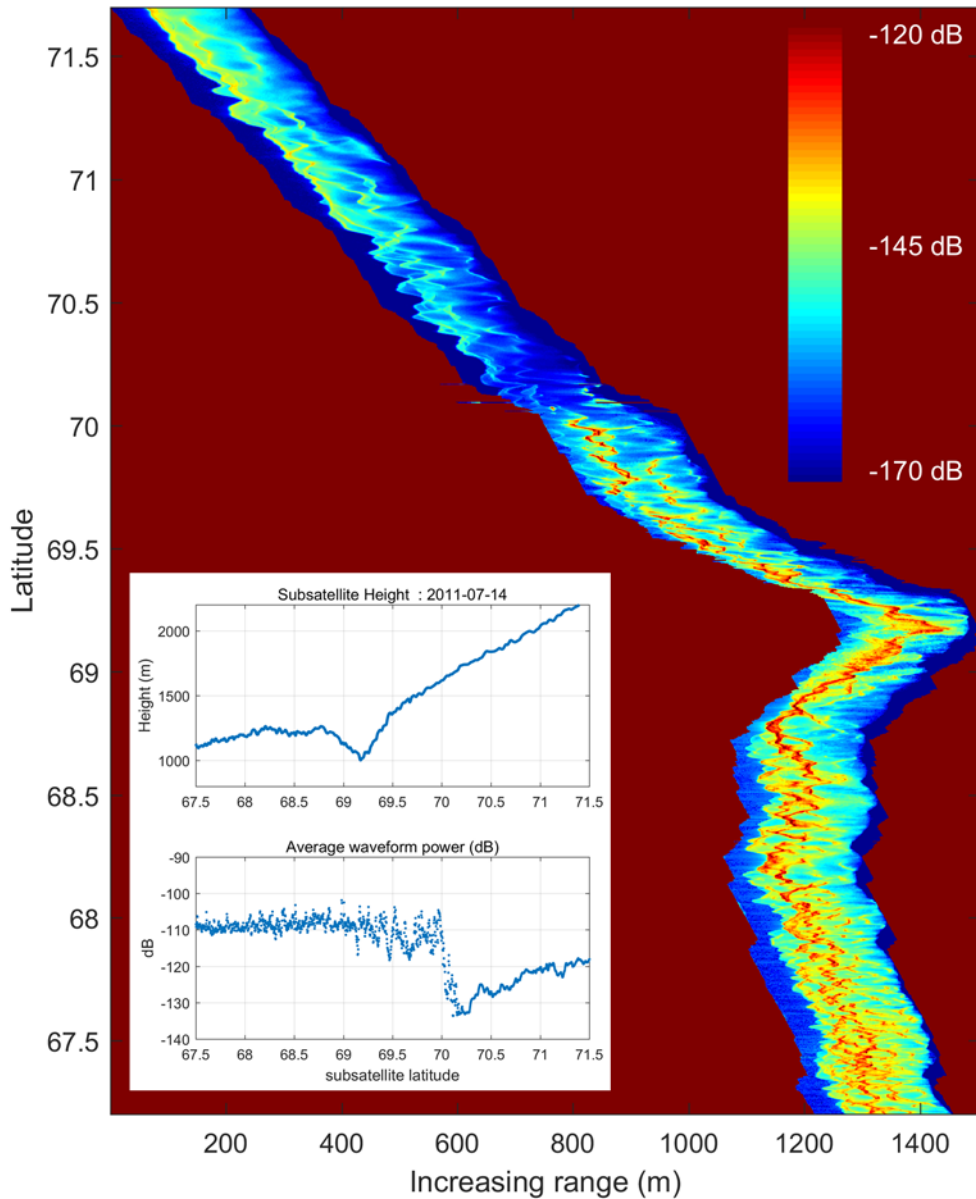
Figure 11. The background image illustrates the swath waveform power in colour with a dB scale for the July 14 2011 descending pass over the west Greenland test area (Fig. 12A). The waveforms making up this pseudo-image have been shifted in the x direction to account for the changing delay time to the first sample and the varying satellite height above the WGS84 ellipsoid. The insert shows the sub-satellite terrain elevation and the waveform average power both plotted against latitude.
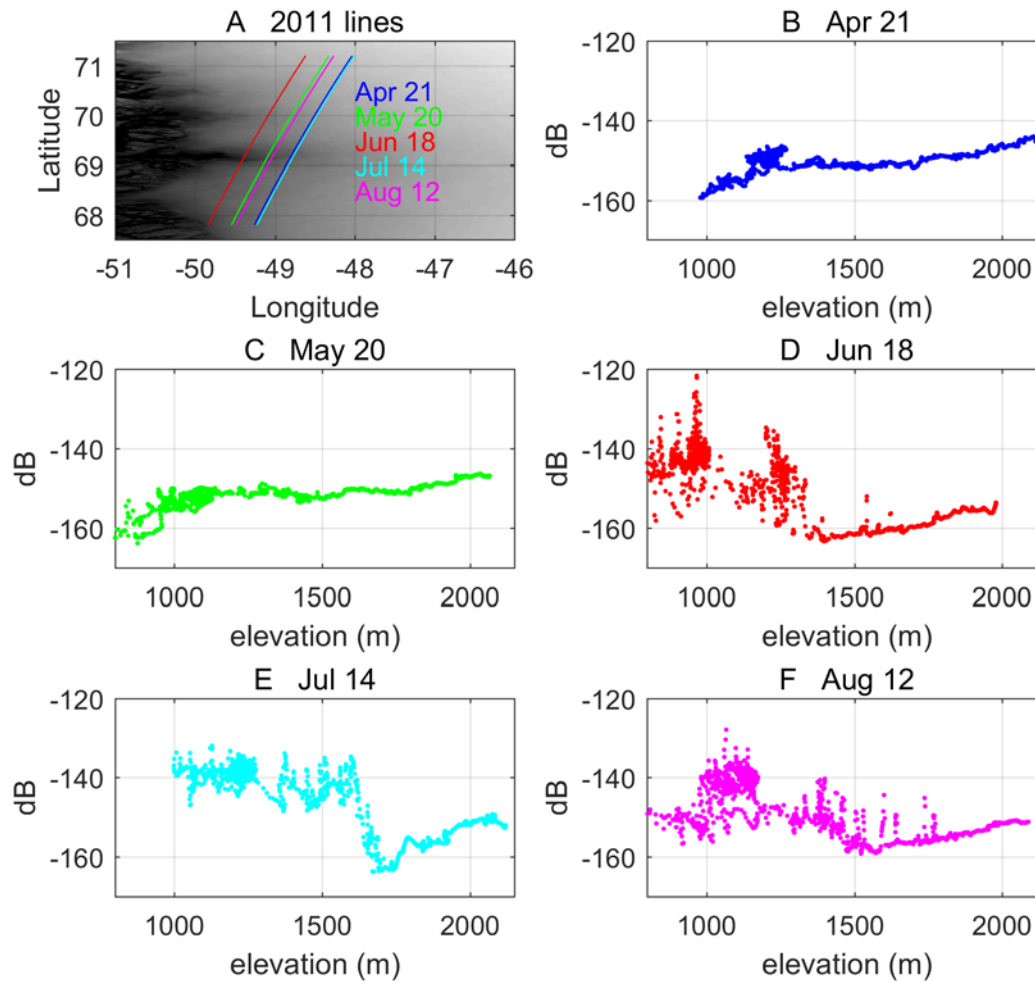
Figure 12. Plots of the average waveform power for the five 2011 descending passes shown in (A). The five plots are from descending passes on (B) April 21, (C) May 20, (D) June 18, (E) July 14 and (F) Aug. 12, and illustrate average waveform power as a function of elevation.
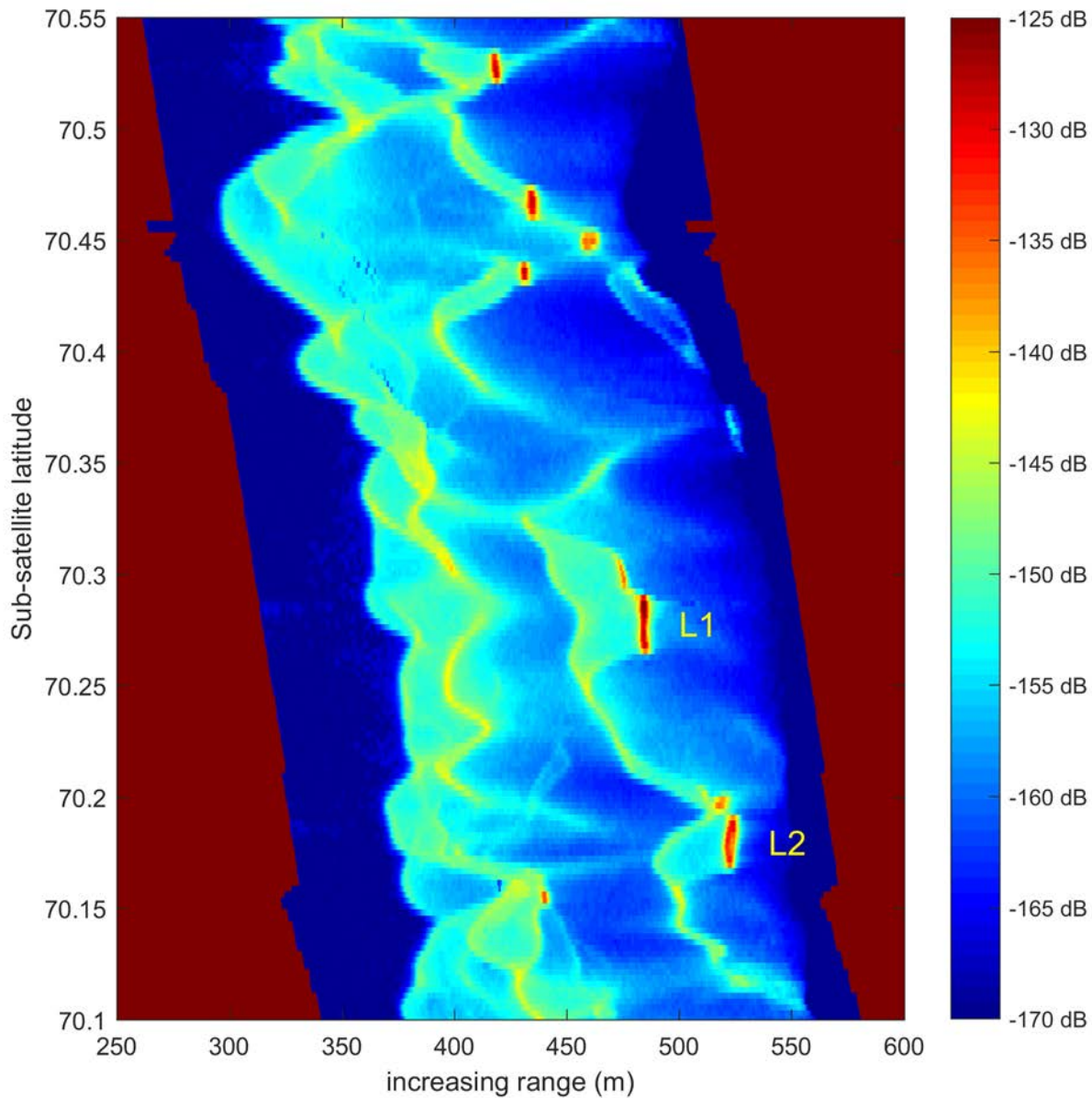
Figure 13. Illustration of part of the waveform power from an ascending pass over west Greenland on 7 August 2011 (Fig. 14). The bright returns labelled as L1 and L2 are at elevations ~ 1609 m and 1573 m, respectively, and represent topographic lows where water could collect.
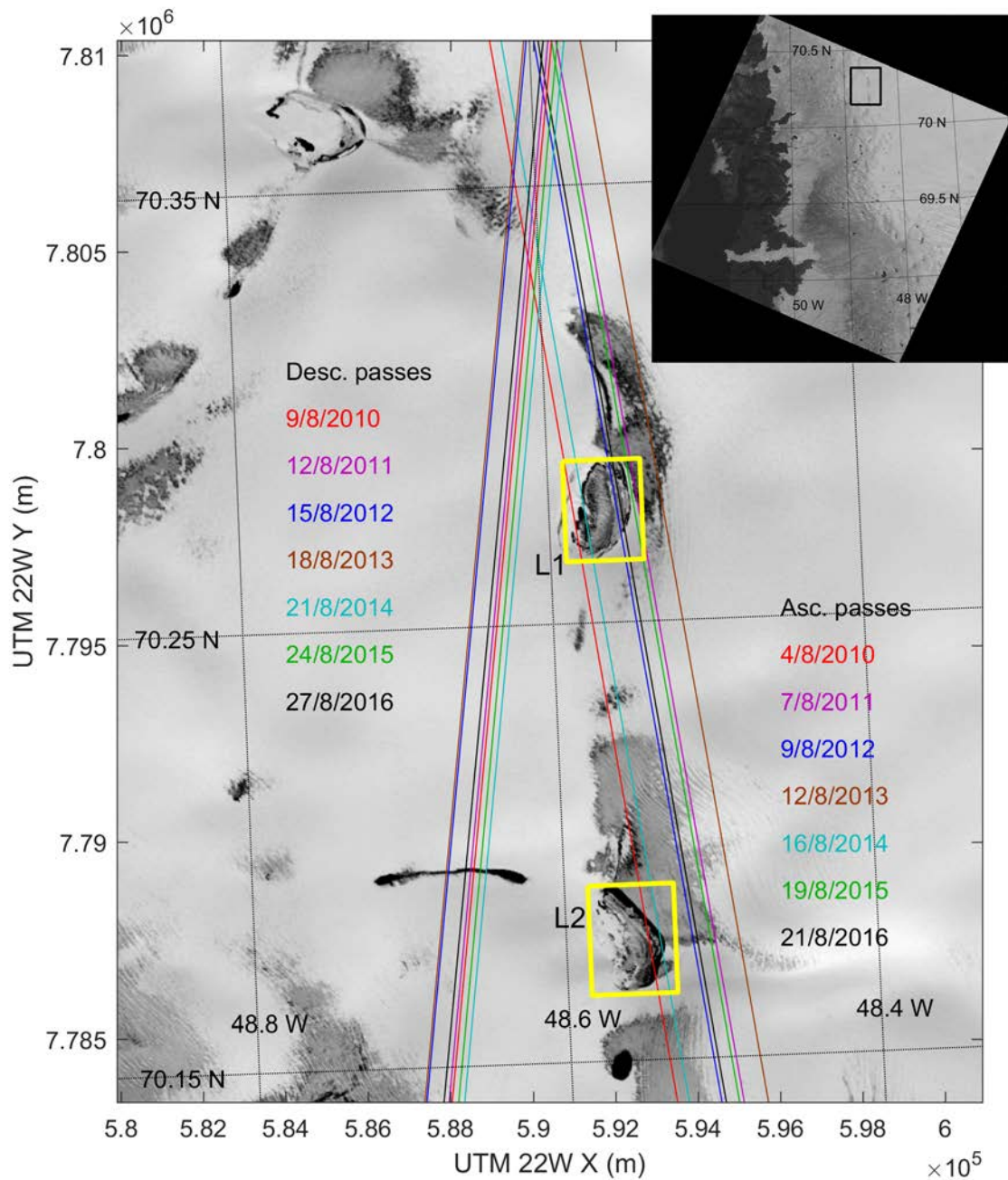
Figure 14. Ascending and descending sub-satellite repeat tracks over, or close to, the L1 and L2 features for all the years from 2010 to 2016 superimposed on part of the Landsat 8 image of August 9 2016 (inset image).
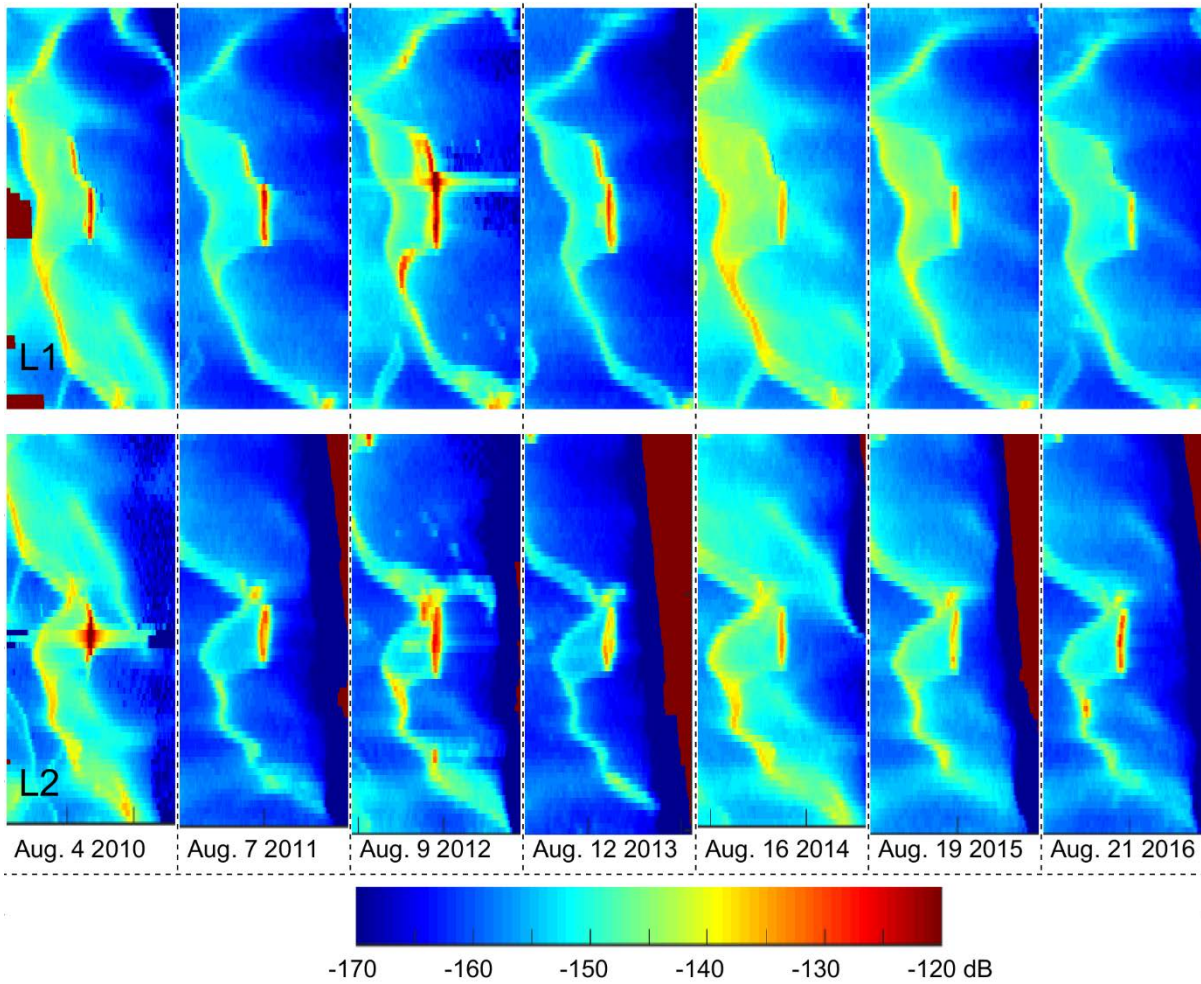
Figure 15. 'Images' of part of the CryoSat waveforms for the areas including 'L1' (top) and 'L2' (bottom) in west Greenland for the August dates in each year from 2010 to 2016. The x and y axes of each 'image' are increasing range and increasing along-track position (North up).
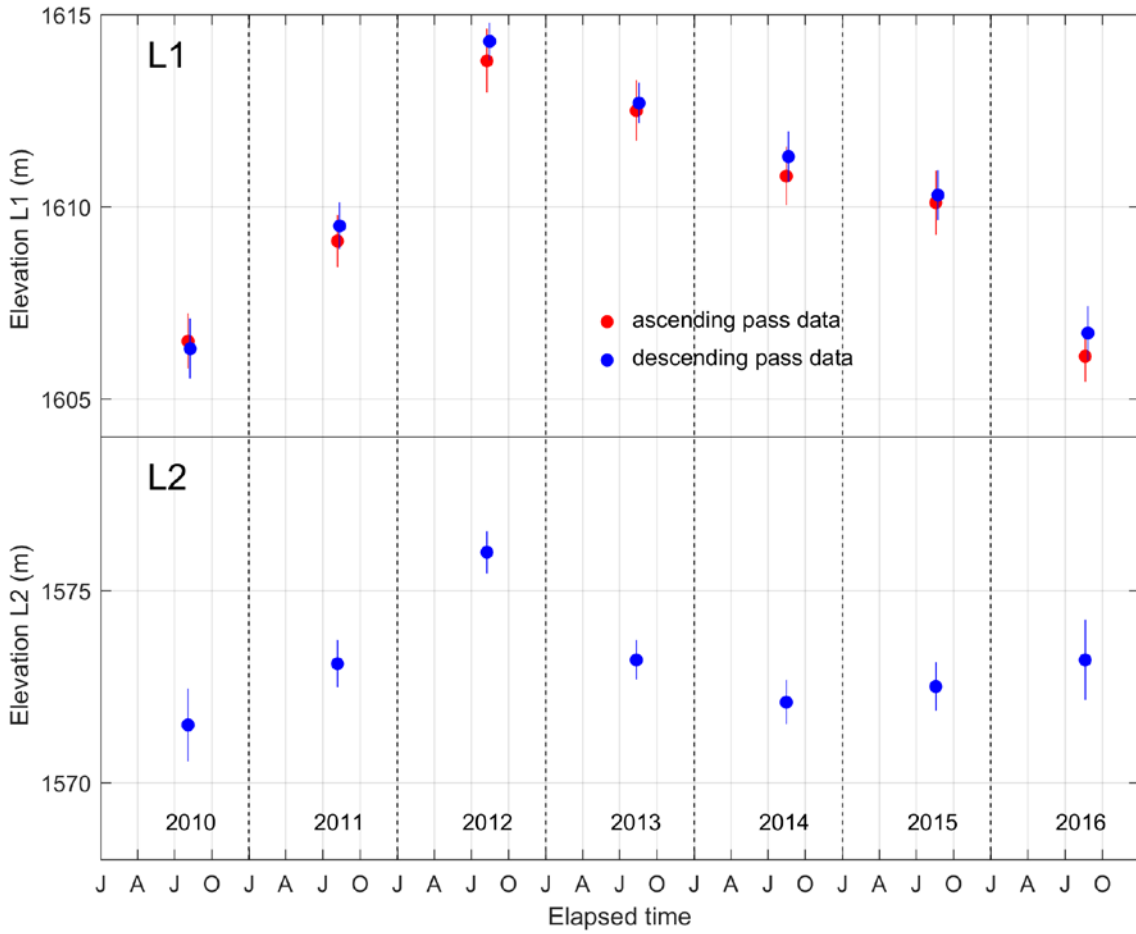
Figure 16. Surface elevation of L1 (top) and L2 (bottom) between the summers of 2010 and 2016.
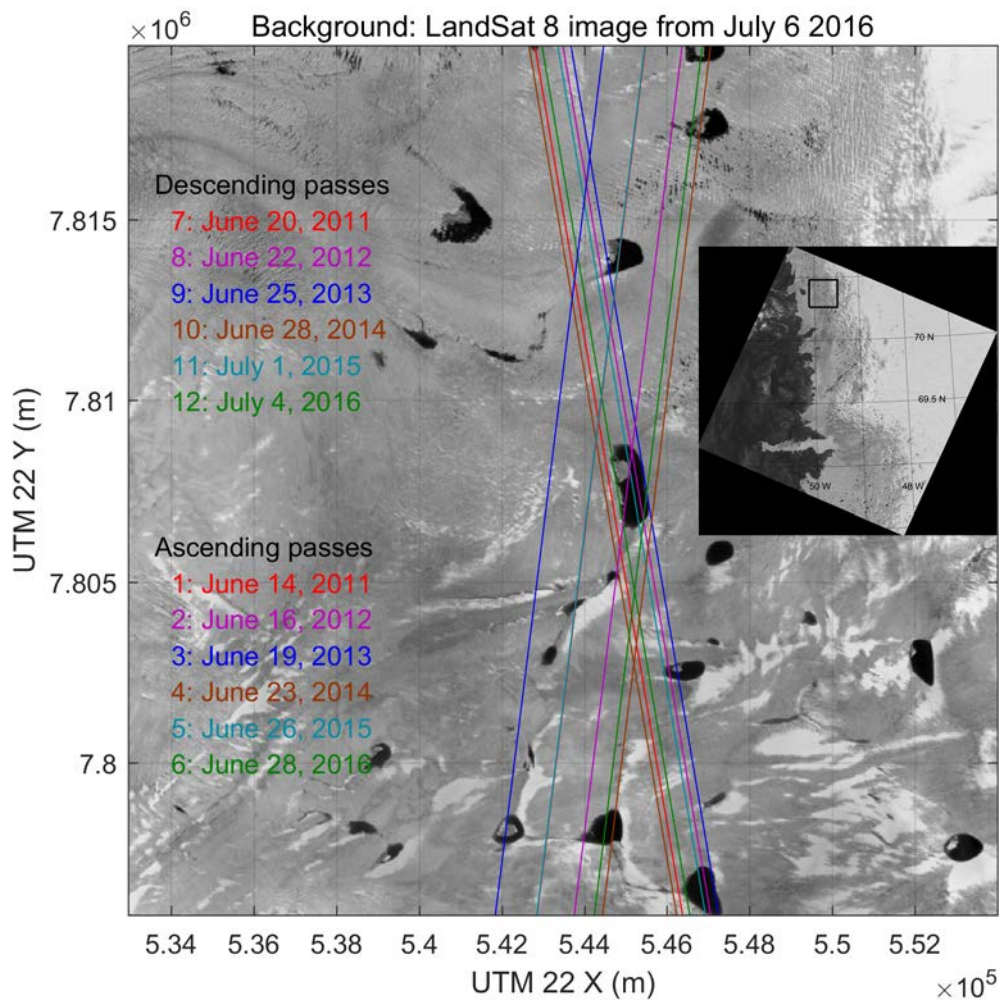
Figure 17. Landsat 8 image from July 6 2016 of an area in the ablation zone of the west Greenland test site which includes a lake (white arrow) viewed by CryoSat on all the repeat ascending and descending passes listed on the image. The insert image shows the blow-up position in the full Landsat 8 frame.
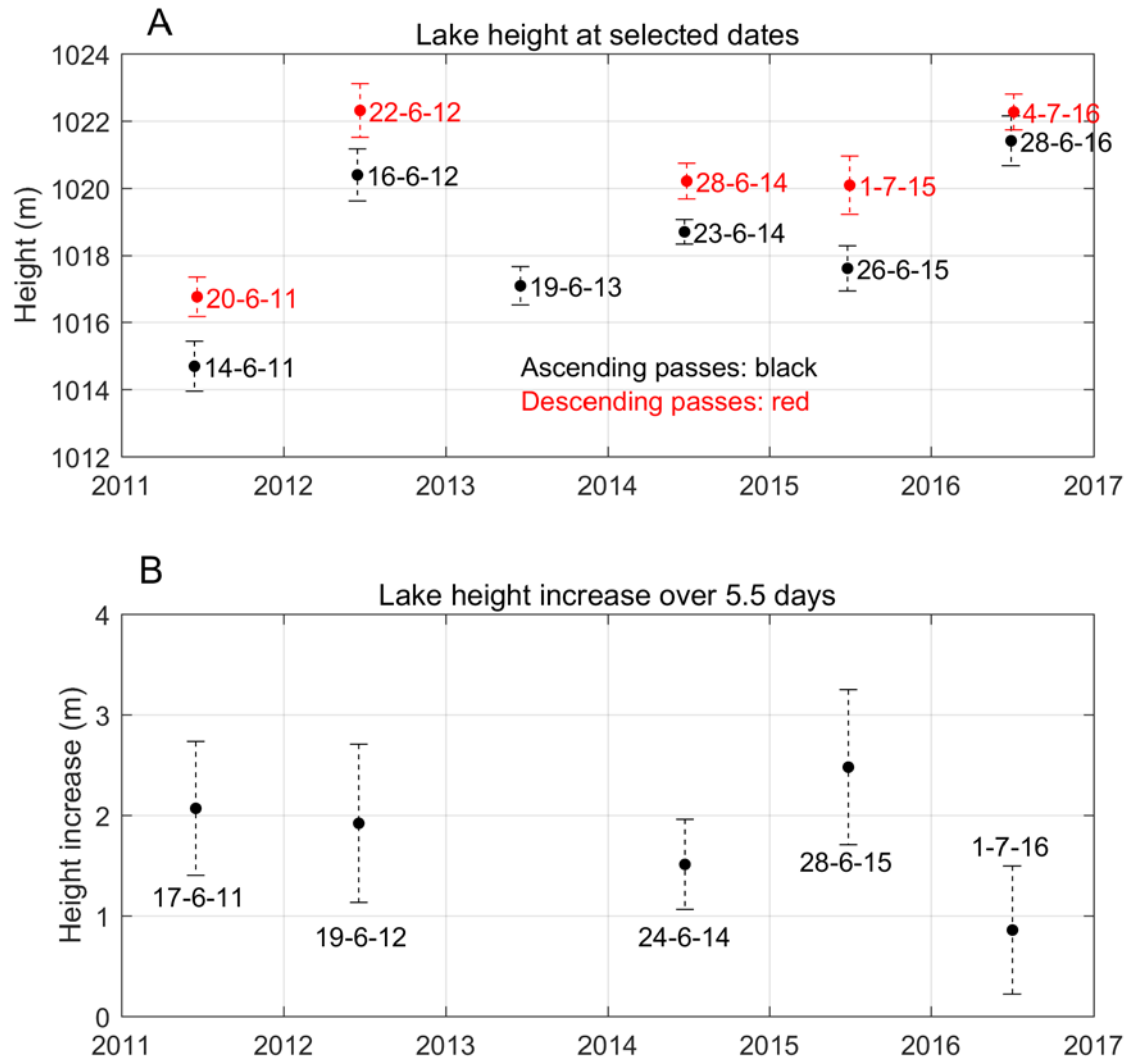
Figure 18. (A) Surface height of the lake in Fig. 17 at the times of the overpasses: (B) Height increase during the 5.5 days between the ascending and descending passes. The dates listed in the lower plot are at the middle of the 5.5-day period between the ascending and descending passes.